CHAPTER 20
HEIGHT FINDING AND 3D RADAR

David J. Murrow
General Electric Company

20.1 HEIGHT FINDING RADARS AND TECHNIQUES

Early Radar Techniques for Height Finding. Early radar techniques employed to find target height were classified according to whether or not the earth's surface was used in the measurement. The practice of using the earth's surface for height finding was quite common in early radar because antenna and transmitter technologies were limited to lower radio frequencies and broad elevation beams. The first United States operational shipborne radar, later designated CXAM and developed in 1939 by the U.S. Naval Research Laboratory (NRL), used the range of first detection of a target to estimate its height, based on a knowledge of the shape of the pattern near the horizon due to the primary multipath null. Later a refinement was made as the target traversed the higher-elevation multipath nulls or "fades." This technique, illustrated in Fig. 20.1*a*, was extensively employed on early shipborne radars, where advantage could be taken of the highly reflective nature of the sea surface. Of course, the technique was limited in performance by such uncontrollable factors as sea state, atmospheric refraction, target radar cross section, and target maneuvers.[1,2]

Reflections from the earth's surface were also used by other early contemporary ground-based radars, such as the British Chain Home (CH) series, which was employed in World War II for the defense of Britain. This radar was a pulsed high-frequency (HF) radar which made height measurements by comparing amplitudes of the (multipath-lobed) main beams of a pair of vertically mounted receiving antennas. Conceptualized in Fig. 20.1*b*, the technique was also utilized in early United States radars, notably, the Canadian-built United States radar SCR-588, and the United States–built SCR-527, both based on the British Type 7 radar design.[3]

One of the earliest and perhaps most direct form of radar height finding was to mechanically direct and hold a narrow-elevation-beam antenna pointed toward the target. The elevation angle of the target corresponds to the elevation readout on the antenna mount. In early radar systems employing this technique, an op-

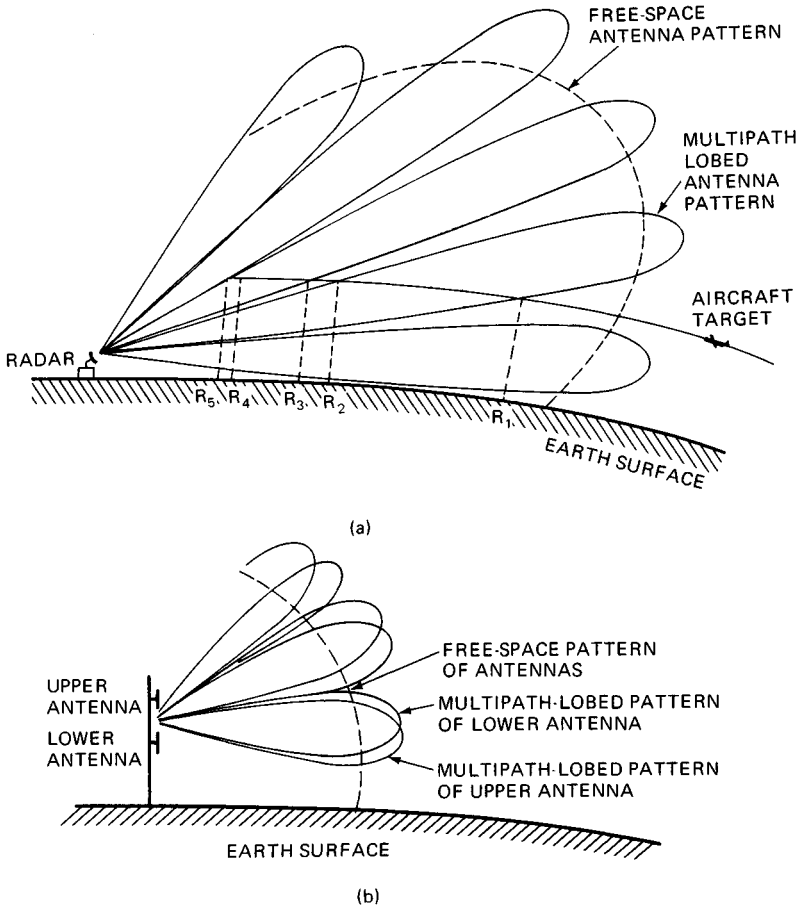

FIG. 20.1 Early radar height finding techniques. (*a*) Method of multipath nulls. (*b*) Amplitude comparison using multipath lobes.

erator would keep the antenna boresighted on the target with a handwheel while monitoring the target return strength. It was quickly learned that maximizing the signal strength of a target echo in a beam was not sensitive enough to provide the desired accuracies, and so alternative techniques were ultimately developed for this purpose. One of the first of these, called *lobe switching*, was first demonstrated in 1937 on a prototype of what later became the U.S. Army Signal Corps SCR-268 radar.[4] This radar was designed for directing antiaircraft gunfire and was the first production radar to use lobe-switching techniques to center the antenna on the target. Two separate identical beams, one above and one below the antenna boresight, are formed at the antenna on receive. By switching between the two beams and keeping the observed amplitudes equal, the SCR-268 elevation operator could keep the antenna boresighted on the target accurately.

If a dish antenna, which generates a narrow pencil-type beam in azimuth and elevation, is mechanically boresighted and trained at or in the vicinity of a target,

allowing determination of its azimuth and elevation, the technique is called *searchlighting*. The searchlight technique was successfully employed on the British CMH radar and on the widely deployed United States SCR-584[5] as well as on the United States SCR-615 and the U.S. Navy SM radar. All these radars were S-band dish antenna radar systems. Some of these dish antennas employed conical scanning of a single beam to provide the elevation error signal required to accurately center the beam on the target. The accuracy of such a technique is very good but obviously is limited to one target at a time. Conical scanning and lobe switching are special cases of a general technique for developing off-boresight error signals called *sequential lobing*. The fundamental accuracy and limitations of the sequential-lobing technique are presented in Sec. 20.3. The searchlighting technique was the forerunner of modern-day tracking radars discussed in Chap. 18, many of which now employ monopulse techniques to develop off-boresight error signals. Obviously, techniques which require the antenna to be boresighted on the target are limited in simultaneous surveillance and height finding capability. Typically they make a measurement on a single target at a time and usually also require a designation at least in range and azimuth by an accompanying search radar. The concept of searchlighting and lobe switching is illustrated in Fig. 20.1*c*.

A widely used early radar dedicated to finding the height of a target in augmentation of a 2D surveillance set was the nodding antenna.* In this type of radar a horizontal fan beam, with a narrow elevation beamwidth, is mechanically scanned in elevation by rocking or "nodding" the entire antenna structure (Fig. 20.1*d*). As the radar beam traverses the target continuously transmitting pulses, the main-lobe target echoes that return are displayed to an operator by means of a range-height-indicator (RHI) type of display. This allowed the operator to precisely and directly estimate the target height of the target by a process termed *beam splitting*, referring to the process of estimating the center of the displayed target video. Although some nodding-antenna height finders had a slow azimuth rotation search mode, most relied on designations of azimuth from an operator. The operator would observe a detection by the 2D surveillance radar and then command a height determination by the height finder. The height finder would then slew to the commanded azimuth and obtain a height and range measurement. This method of operation was relatively slow and limited in multiple-azimuth target-tracking capability compared with 3D radars. These drawbacks seriously limited the continued use of the manual nodding-antenna height finder in military applications.

Several nodding-antenna height finders, notably the British Type 13 and the widely deployed United States AN/TPS-10, appeared in the mid- to late 1940s, when higher-frequency technology began to emerge.[6] The AN/TPS-10 X-band nodding-antenna height finder radar series was subsequently replaced by the AN/FPS-6, an S-band nodding-antenna radar also designed for the U.S. Army.[7] The AN/MPS-14 was a mobile version of the radar, and the AN/FPS-89 was an improved fixed-site version. The elevation beamwidth of the AN/FPS-6 was 0.9°, its azimuth beamwidth was 3.2°, and the entire antenna nodded at a rate of 20 to 30 nods per minute. The radar could scan in azimuth at a rate of 45° per second. It transmitted 2-μs pulses with pulse repetition frequencies (PRFs) from 300 to 400 Hz, and operated with a peak power of 4.5 MW.

*Nodding-antenna height finders have also been used for raid counting.

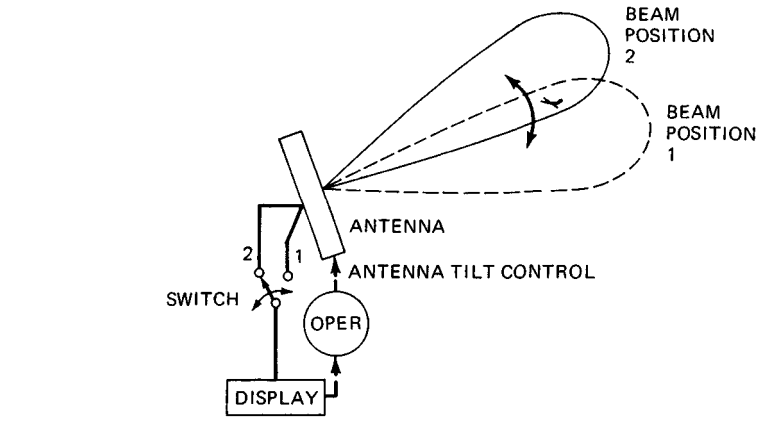

(c)

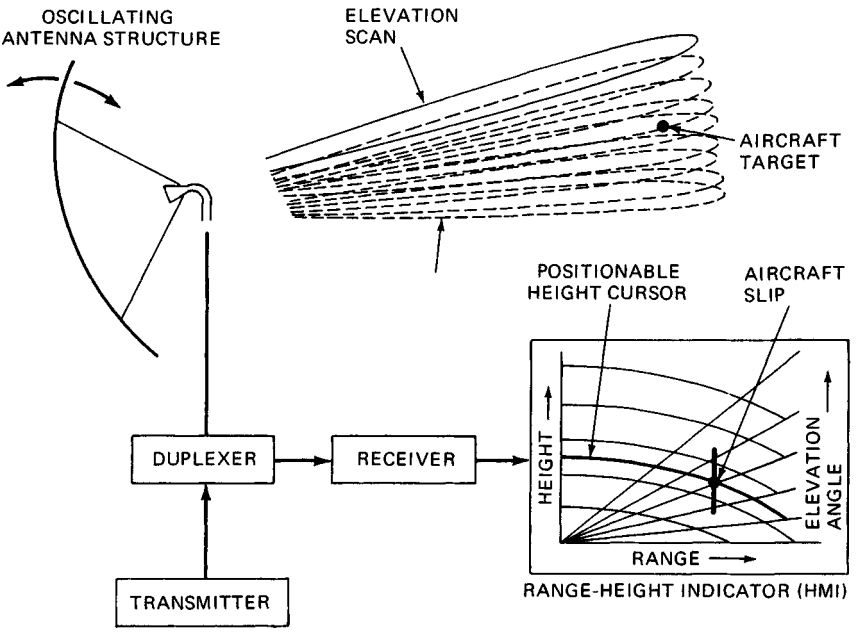

(d)

FIG. 20.1 *(Continued)* Early radar height finding techniques. (*c*) Searchlighting with lobe switching. (*d*) Nodding antenna.

The data rates of later versions of the nodding-antenna radar have been considerably improved over their predecessors. For example, the S600 series C-band nodding-antenna height finder is computer-controlled and -managed for maximum data rate, enabling it to obtain up to 22 height measurements per minute.[8]

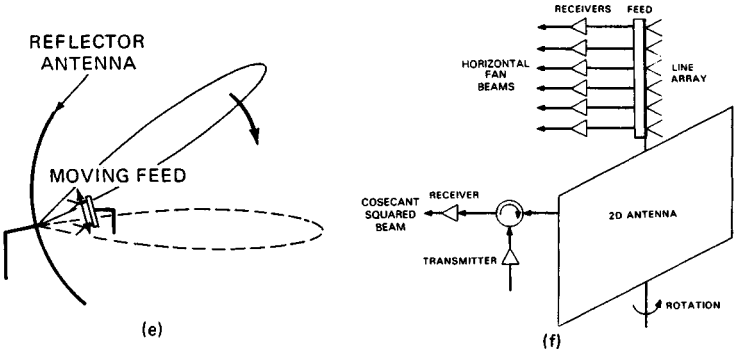

FIG. 20.1 (*Continued*) Early radar height finding techniques. (*e*) Electromechanical beam scanning. (*f*) 2D antenna with vertical line array.

Of course, it is possible to rapidly scan a horizontal fan beam in elevation by electromechanical means (Fig. 20.1*e*) instead of by mechanically rocking the entire antenna structure. Many nodding-beam-type height finders with ingenious means of beam scanning have been successfully deployed over the years. Two notable examples are the World War II SCI radar and the AN/SPS-8 shipborne radar, both of which used a Robinson-type electromechanical feed to rapidly scan the beam in elevation.

The development of higher-frequency microwave technology facilitated electrically larger apertures and correspondingly narrower beams, all in convenient physical sizes. Accompanying this evolution was a series of inventions of rapid electromechanical scanners based on geometric optic principles and developed for surveillance radar applications. These include the Robinson, delta *a* (Eagle), organ-pipe, Foster, Lewis, and Schwartschild scanners, along with a variety of polarization-switching mirror scanners. These scanners all utilized the motion of the feed structure of the antenna to control the incidence of illumination on the aperture, thereby scanning the beam. The reader may refer to a number of excellent sources for a detailed treatment of the method of operation of electromechanical scanners.[6,9,10] In principle, a relatively inexpensive volumetric 3D radar could be created by using an electromechanical feed and scanning a narrow pencil-type beam in elevation while rotating the antenna in azimuth. In practice this approach has not been employed because of the lack of waveform flexibility versus elevation angle imposed by the constant-rate scanning of the electromechanical feed.

During World War II, the British developed a very-high-frequency (VHF) phased array antenna height finder called the Variable Elevation Beam (VEB) radar. This 200-MHz radar utilized mechanically adjustable phase shifters to control the relative phase of nine groups of eight dipoles on a 240-ft mast. The resulting elevation beamwidth was approximately 1° in width and was phase-scanned over an elevation interval slightly more than 6° in extent.

A technique which has seen limited service for radar height finding is a vertical receive-only line array mounted on a conventional 2D surveillance radar as shown in Fig. 20.1*f*. The line array is processed to form a stack of receive horizontal fan beams, each of which is relatively narrow in elevation. Since the (narrow-azimuth) transmit beam is generated by the 2D radar antenna, the resulting stack of two-way beams is narrow in both azimuth and elevation. The stack of

receive beams may be formed in a number of ways from the line array. One technique is the Butler matrix, an RF feed analog of the discrete Fourier transform. A second technique was designed for an experimental version of the FAA AHSR-1 S-band air traffic control.[11] The technique augmented the 2D surveillance aperture with a vertical receive-only line array of elements. Each beam of a vertical stack of horizontal fan beams was generated from the line array by combining energy coupled out of waveguide runs at the appropriate length from the element to produce a linear-phase gradient element to element. This produced a set of uniformly illuminated beams, each time-delay-steered to the desired elevation.

One of the early radars combining 2D surveillance with height finding was the AN/CPS-6B, which utilized the V-beam principle. The V-beam radar consisted of a primary and a secondary antenna aperture mounted on the same rotating shaft. The primary aperture operated as a conventional 2D radar, generating a vertical cosecant-squared fan beam which provided detections and the range and azimuth coordinates of targets in the surveillance volume. The secondary antenna aperture was similar to the primary aperture except that it rotated about an axis normal to the aperture. This produced a second fan beam which was tilted from the vertical plane. The two beams might be powered by the same or separate transmitters, but each beam had its own receiver. The tilted beam provided a second set of detections to the radar operator as the antenna rotated. The azimuth separation of the center of the two sets of detections corresponding to a single target, correlated by the operator using range, was directly proportional to the height of the target, to within flat-earth and normal propogation approximations. The concept of the V-beam radar is illustrated in Fig. 20.1*g*.

The V-beam radar has been referred to as a 3D radar by some authors.[3,7,10] Technically, however, it should not be classified as a true 3D radar because it lacks resolution in the elevation dimension. This shortcoming limits its use to low-density aircraft situations where it is unlikely to encounter two aircraft appearing at the same range and azimuth but at different heights.

The Japanese have developed a radar based on phase interferometry to find height in air traffic control applications,[12] but it also does not have resolution in the elevation dimension. The concept employs a set of four horizontal line arrays vertically displaced in a staggered fashion about a conventional 2D reflector-type antenna. The principle utilized by phase interferometry is that the phase difference between offset antennas is proportional to the sine of the angle of arrival of a received target echo as sketched in Fig. 20.1*h*.

Radars such as the VEB, the V-beam, the vertical line array plus 2D, the crossed-line array, and the phase interferometer plus 2D, which obtain simultaneous tricoordinate (range, azimuth, and elevation or height) measurements on a target but do not have significant resolution in the elevation dimension compared with their elevation coverage, might appropriately be termed 2½D radars.

Height Finding Techniques in 3D Radars. There are many types of radars that provide 3D information by simultaneously measuring the three basic position coordinates of a target (range, azimuth, and elevation). In this handbook, however, the convention is followed in which a *3D radar* is taken to be a surveillance radar whose antenna mechanically rotates in azimuth (to measure range and azimuth) and which obtains the elevation-angle measurement either by scanning one or more beams in elevation or by using contiguous, fixed-elevation beams.

Military interest in 3D radar stems from its ability to determine the height of a noncooperating target, along with its range and azimuth. Because of its better angu-

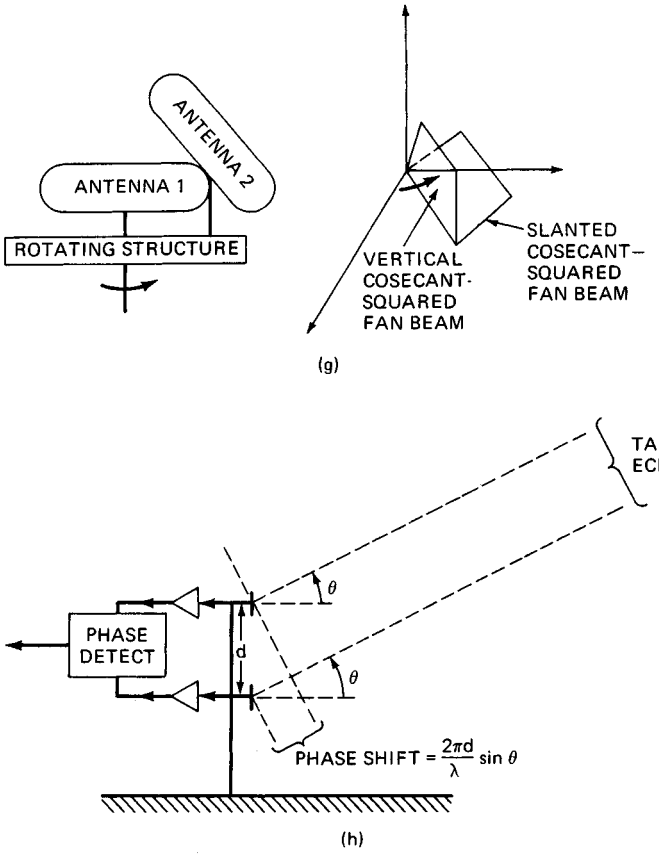

FIG. 20.1 *(Continued)* Early radar height finding techniques. (*g*) V-beam radar. (*h*) Phase interferometry.

lar resolution the 3D radar provides a higher-gain antenna and, arguably, a greater resistance to jamming and other forms of electronic countermeasures (ECM) than a combination of 2D and dedicated height finder. The counterargument points out that the 2D and height finder may be implemented in two separate frequency bands, forcing the jammer to spread out its energy, thereby diluting it.

Rotating 3D radars can be implemented as stacked-beam radars, frequency-scanned radars, phase-scanned radars, electromechanically scanned radars, and digital beamforming radars, according to how the elevation beams are formed and/or scanned in elevation.

Stacked-Beam Radars. Stacked-beam radars employ a vertical *stack* of simultaneously formed receive beams in elevation which are mechanically rotated in azimuth in order to perform search and tricoordinate target position estimation. The target is illuminated by a single transmit beam which is broad enough to cover the receive beam main lobes containing the target. Elevation-angle estimation may be accomplished in such a radar by an amplitude comparison technique, by which the amplitudes of the return at the target range in two or more adjacent

simultaneous elevation receive beams are compared. The technique is thus a special case of the general technique of simultaneous lobing. Target height is determined via computer table lookup, using range and elevation entries. The sensitivity of this approach depends on the relative spacings of the beams in the stack, the aperture illumination used to form the beams, and the elevation angle of arrival of the target relative to the beam boresight placements, along with other equipment-related error sources.

It should be noted that the overall height finding performance of a stacked-beam radar is greatly influenced by the extent to which the designer includes anticlutter moving-target indication (MTI) and/or doppler processing in the beam stack, even in clear weather conditions. This is especially important for the lowest beam in the stack, as its main lobe intercepts the earth's surface, admitting surface clutter returns. However, it may also be important for all the beams in the stack, depending on the severity of the clutter. This is so because the elevation patterns of a stacked-beam radar are primarily one-way patterns, being dominated by the receiver elevation pattern. Thus, the elevation sidelobes protecting the radar upper beams from ground or sea clutter are the (one-way) elevation receive sidelobes. This is true because the transmit beam main lobe must be broad enough in elevation to cover all receive beams. This is different from the scanning pencil-beam radar, in which the product of the transmit and receive elevation sidelobes protects the radar upper beams from surface clutter. In benign surface clutter applications, it is economical to implement the stacked-beam radar without MTI or doppler processing in the beam stack, reserving this processing for a single cosecant-squared receive detection beam.

The AN/TPS-43 is an example of a widely deployed operational stacked-beam radar. Deployed in the 1970s, it is a transportable ground-based S-band radar which has been extensively used for air surveillance in the U.S. Air Force Tactical Air Command System (TACS). The radar employs a multiple-horn feed illuminating a reflector-type antenna rotating at 6 r/min to generate a stack of six receive beams in elevation. The original version of the radar utilized a linear-beam Twystron tube to generate approximately 4 MW of RF peak power in a 6.5-μs simple pulse. The radar is instrumented to a range of 240 nmi and operated with six PRFs averaging 250 Hz. The receive beams in the stack are 1.1 in azimuth and variable in elevation beamwidth in such a way that the six span the 20° of total elevation coverage. Subsequent versions of the radar provided pulse compression and improved MTI waveforms and processing.[13] The AN/TPS-75 is an upgraded version of this radar with a planar array low-sidelobe antenna.

Another example of a stacked-beam radar is the S713 Martello (Fig. 20.2*a*), an L-band transportable radar with an eight-beam stack. The Martello S713 radar employs IF processing to form the receive beam stack in elevation. In operation, a cosecant-squared transmit beam is formed and eight narrow beams are formed and processed on receive. A ninth receive beam, cosecant-squared in shape, is used for surveillance and detection. Azimuth and range are determined as in a conventional 2D radar. Height finding is accomplished by interpolating the received signal strengths in adjacent elevation beams of the stack to determine the target elevation angle. The array is 10.6 m high by 6.1 m wide and consists of 60 center-fed rows of 32 radiating elements, each equipped with 60 receivers to downconvert received RF to IF. The azimuth beam is 2.8° wide. The tube transmitter generates 3 MW of RF power at the peak of a 10-μs pulse and an average RF power of 8 kW. The radar is instrumented to 256 nmi and up to 30° in elevation and 100 kft in height. The antenna rotates at 6 r/min. A height accuracy of

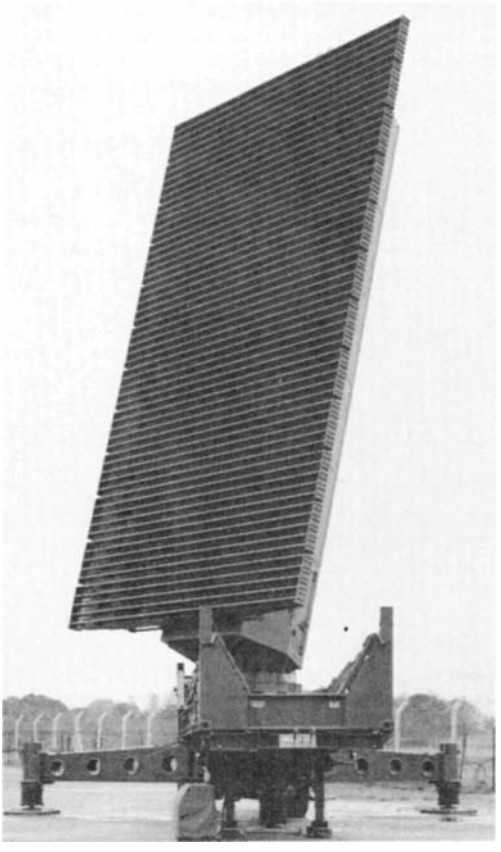

(a)

FIG. 20.2 Exemplar 3D radars. (*a*) S713 Martello stacked-beam 3D radar (*Courtesy Marconi Company*).

1000 ft on a small fighter aircraft at 100 nmi is claimed by the radar manufacturer. A solid-state transmitter version of the radar, the S273 with a shorter and wider array, is also available. This version offers a six- or eight-beam stack, with a 1.4° azimuth beamwidth but with wider beams in elevation covering to 20° total elevation. The solid-state transmitter consists of up to 40 modules generating 132 kW of total RF power at the peak of a 150-μs pulse and up to 5 kW of average power. The height accuracy claimed for the radar by its manufacturer is 1700 ft on a small fighter at 100 nmi.[14]

A radar which is a hybrid mix of stacked beams and phase steering is the RAT-31S, an S-band radar which phase-steers a stack of four beams in elevation to cover the surveillance volume. The radar employs monopulse to determine target height. It rotates a 13.2-ft-square array at 5 to 10 r/min while generating a stack of three receive beams covering 21° in elevation. The array is divided into three vertical sections. Each section of the array then generates its own beam, which is phase-steered over a designated section of the elevation coverage.[15]

Scanning Pencil-Beam Radars. Another method of achieving 3D volumetric coverage suitable for high-air-traffic situations is the scanning pencil-beam radar. The most common radars in this class obtain high volumetric coverage by employing an antenna feed technique which electronically scans a narrow pencil-type beam through the elevation coverage as it rotates in azimuth, producing an azimuth-elevation scanning pattern similar to that of a TV raster scan.

For the air volume surveillance mission, electronic scanning provides flexibility and performance not readily available in electromechanical scanners. These advantages include (1) shorter volume surveillance frame times; (2) highly flexible computer-programmable waveform versus elevation time and energy management; (3) electronic compensation for moving platforms and mobile applications such as ground vehicles, ships, and aircraft; and (4) wide and flexible elevation coverage, including highly agile beam placement in elevation, programmable elevation coverage versus range and azimuth, good beam shape preservation over wide coverage, and flexible, precise control of beam placement versus azimuth, which is especially critical for low-elevation-beam performance.

Frequency Scanned Radars. One of the earlier 3D radar techniques that has found application for the air surveillance mission is frequency scanning. Frequency-scanned arrays utilize the frequency-dependent phase characteristics of a length of transmission line, usually waveguide, to scan a pencil beam.[16] The waveguide is folded into a serpentine configuration on the side (or sides) or back of the array to provide output taps at the locations of the closely spaced antenna elements. A controlled change of transmit/receive RF frequency produces a different phase gradient across the aperture, electronically steering the beam to the desired elevation angle. Frequency scanning may be accomplished from pulse to pulse by changing the transmitter and receiver frequency sequentially from one pulse to the next, or "within" the pulse, by transmitting a chirp linear-frequency-modulated (LFM) pulse or sequence of contiguous subpulses each stepped in frequency, and by processing each of a stack of receive beams in elevation each at one of the subpulse frequencies.[17] The AN/SPS-39 S-band shipborne radar used a parabolic-cylinder reflector antenna fed by a line source to produce the change in phase with frequency necessary to scan its beam electronically in elevation. Upgraded with a planar array, this radar evolved into the AN/SPS-52[18] (Fig. 20.2*b*). The within-pulse approach was employed on the AR3D S-band surveillance radar. It transmits LFM pulses and extracts the target height via frequency discrimination in the receiver.[19]

The U.S. Marine Corps AN/TPS-32, the U.S. Navy shipborne AN/SPS-48, and the Series 320 radars are all examples of S-band 3D surveillance radars consisting of a small stack of frequency-scanned beams which are then step-scanned as a group to cover the elevation surveillance volume.[20,21]

The use of frequency-scanning beams in elevation as a height finding technique is a form of the general technique of sequential lobing, in which amplitudes from adjacent sequentially formed beams are compared to estimate the target elevation angle. The elevation-angle accuracy achievable in this class of radars is not as good as that of stacked-beam or phase-scanned monopulse radars, e.g., radars employing simultaneous lobing. There are several fundamental reasons for this. One is that because different frequencies are required in order to steer the beam, amplitude fluctuations in the target return are induced. These tend to dilute the quality of target angle information available in the multiple-beam target returns. The effect can be compensated by averaging out the target fluctuation effects by the use of noncoherent integration of multiple-frequency diversity subpulses in each beam. However, the diversity subpulse frequency separations

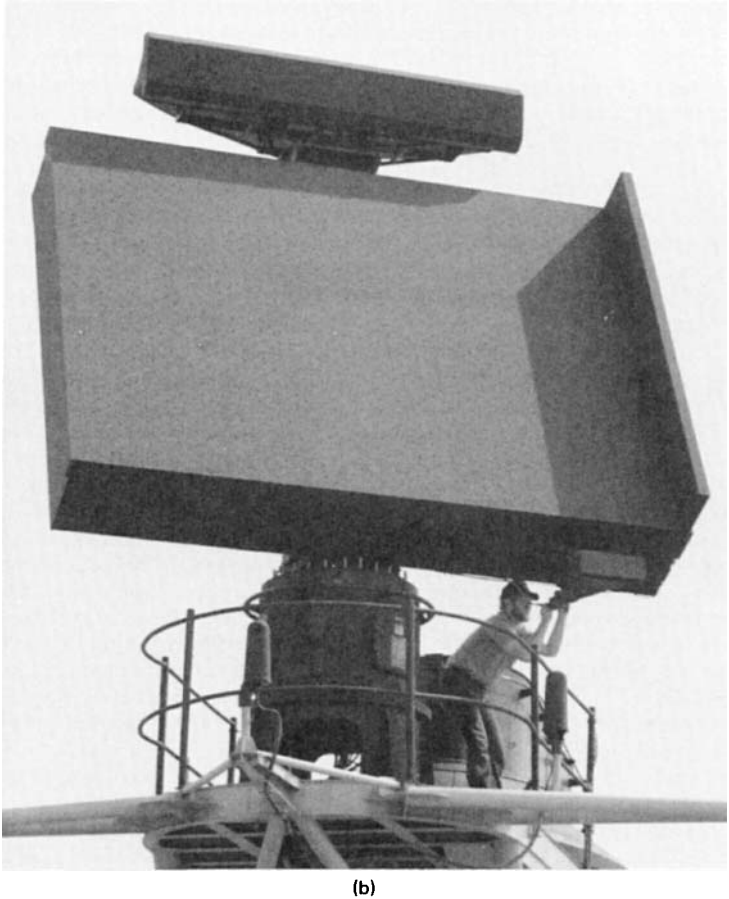

(b)

FIG. 20.2 *(Continued)* Exemplar 3D radars. (*b*) AN/SPS-52C shipboard frequency-scanned 3D radar (*Courtesy Hughes Aircraft Company*).

must be enough to induce target amplitude fluctuations while not causing too much beam steering—a difficult tradeoff in some applications. Sequential-lobing angle estimation techniques are also vulnerable to time-varying or amplitude-modulation jammers such as blinkers. The fact that RF frequencies correspond one to one with elevation angle in the frequency-scanned radar constrains it in the use of frequency agility for electronic counter-countermeasures (ECCM) purposes. It also tends to limit its flexibility in waveform time and energy management. The electronically steered phased array provides considerable relief to the designer from these limitations.

Phased Array Radars. Scanning or steering of a pencil-type narrow beam in elevation can be accomplished by means of electronically controlled phase shifters placed at the row feed outputs of an array antenna. This approach is the most flexible of the various 3D radar height finding techniques, allowing full use of the frequency band for purposes beyond beam scanning and allowing for com-

plete independence of waveform and beam position. Height finding techniques which can be used with the phase-scanned array include a variety of coherent simultaneous-lobing (monopulse-multipulse* and phase-interferometry) techniques, as well as amplitude comparison sequential-lobing techniques. The phased array radar is becoming more commonplace in the present-day military marketplace, owing to an ever-escalating target and threat environment and dynamics.

The AN/TPS-59 L-band radar is an example of a long-range transportable 3D tactical radar with phase scanning to steer the beam in elevation. Developed for the U.S. Marine Corps, it is unique among air surveillance radars in that it was the first to employ an all-solid-state transmitter. The solid-state transmitter of this radar is distributed over the antenna aperture in the form of individual row transmitter units. The total transmit power is combined only in space, in the far-field collimated beam. The planar array antenna consists of 54 rows of horizontal stripline linear arrays. Each of the 54 rows contains its own solid-state modular transceiver consisting of a 1-kW nominal RF peak-power solid-state transmitter, integral power supply, low-noise receiver, phase shifter, duplexer, and logic control, all mounted on the antenna. The feed structure of the 15-ft by 30-ft planar array generates a full two-axis monopulse beam set on receive, consisting of a sum and two delta beams. An additional column feed provides a special low-angle height finding capability for the lowest angle beam positions. The feed generates a pair of squinted sum-type beams carefully placed in elevation and processed as a monopulse pair. The technique minimizes the effects of multipath. Its fundamental accuracy performance is considered in Sec. 20.3. The 1.6° by 3.2° monopulse beam set is electronically phased-scanned from −1 to 19°.[22–24] Fixed-site variants of this radar are the AN/FPS-117 SEEK IGLOO radar (Fig. 20.2*c*) and the GE-592 radar, both of which are distributed aperture solid-state and similar to the AN/TPS-59 but which employ a 24- by 24-ft array antenna with 44 rows and additional digital signal processing. The square-aperture array of the GE-592/FPS-117 radar generates a 2.2° azimuth by 2° elevation two-axis monopulse beam set.[25–28]

The HADR, deployed mainly in Europe for North Atlantic Treaty Organization (NATO) applications, is a ground-based 3D S-band phased array radar which also uses phase scanning in elevation and mechanical rotation in azimuth. The radar's 12.5-ft by 16-ft planar array rotates at 5 r/min while phase-scanning a single pencil-type 1.45° azimuth by 1.9° elevation beam through 12 long-range search beam positions and 4 MTI beam positions in elevation. The instrumented coverage of the radar is 250 nmi in range, 20° in elevation, 360 degrees° in azimuth, and 120 kft in height. Target height is estimated by using sequential lobing between contiguous beams in elevation.[29]

A significant example of a long-range airborne 3D surveillance radar is the AWACS (Airborne Warning and Control System) AN/APY-1 S-band radar used on the E-3A aircraft. Because of the limited vertical aperture extent of the AN/APY-1 radar, the elevation beam is relatively broad. Consequently the height accuracies achieved by the radar do not compare well with those of its surface-based counterparts.

*The term *multipulse* is used by the author to refer to a target angle estimation technique discussed in Sec. 20.3 for coherently combining received monopulse sum- and delta-channel (I,Q) target echo samples from multiple-pulse transmissions. This technique is to be distinguished from the combining of individual monopulse angle measurements from each of the multiple-pulse transmissions.

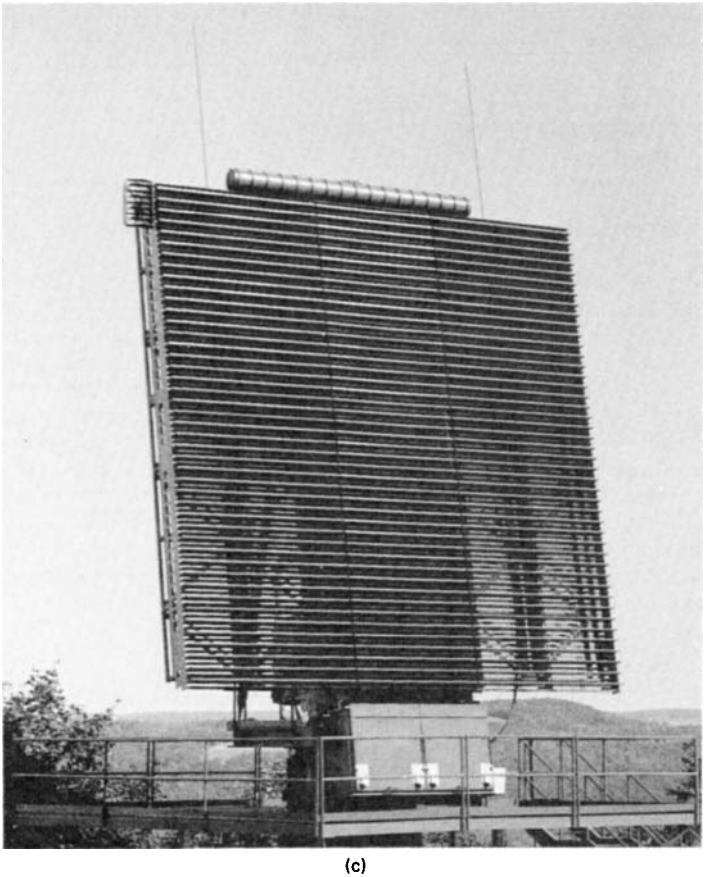

(c)

FIG. 20.2 *(Continued)* Exemplar 3D radars. (*c*) AN/FPS-117 fixed-site solid-state phase-scanned 3D radar (*Courtesy General Electric Company*).

Digital Beamforming Radar. A technology with considerable attractiveness for radar is digital beamforming. As a technique for finding target height, digital beamforming involves placing a receiver on each element of a vertical array of elements, or rows of elements. By digitally weighting and linearly combining the analog-to-digital (A/D) converted receiver outputs, a stack of receive beams or a single scanning receive beam in elevation can be generated. In this form, a digital beamforming radar is a special case of a stacked-beam radar, implemented in a technology that offers several advantages over conventional stacked-beam technology. The major advantage offered by digital beamforming technology is that of full adaptive control of the beam patterns for ECCM purposes. The major challenge faced by digital beamforming radar designers relative to height finding is to develop techniques to preserve monopulse ratios in the presence of adaptive array cancellation of jamming, including those in the main lobe. Monopulse beam pairs or stacked beams are easily generated digitally, but the accuracy of height

finding depends on a precise, unambiguous knowledge of the relative patterns of the (adapted) height finding beams.

20.2 DERIVATION OF HEIGHT FROM RADAR MEASUREMENTS

Height in radar is always a derived rather than a measured quantity. This is true because a radar can only measure range and angle of arrival of target returns. Surface-based radars derive the height of a target from the range (time) of the echo return and elevation coordinate measurements. A radar on a ship, aircraft, or space satellite may be required to convert tricoordinate measurements relative to the antenna to an inertial reference system as part of the height calculation. The accurate calculation of height from radar measurements must provide for such effects as the location and orientation of the radar antenna in the desired reference coordinate system, the curvature of the earth, the refractive properties of the atmosphere, and the reflective nature of the earth's surface. Furthermore, if the target height is to be referenced to the local terrain, then the height of that possibly irregular terrain below the target must also be taken into account. The effects of some of the systematic internal equipment errors can also be partially offset by incorporating internal calibration measurements into the range and angle estimation algorithms.

Flat-Earth Approximation. For very-short-range targets, a sufficiently good estimate of target height is given by the flat-earth approximation:

$$h_T = h_a + R_T \sin \theta_T \tag{20.1}$$

where h_a is the radar antenna height, R_T is the measured target range, θ_T is the measured or estimated target elevation angle, and h_T is the estimated target height.

Spherical Earth: Parabolic Approximation. A somewhat better approximation to target height which models the earth's curvature as parabolic in range can be derived by reference to Fig. 20.3*b*. For a radar located near the surface of the earth, it can be readily shown from the law of cosines that, to a first approximation,

$$h_T = h_a + R_T \sin \theta_T + R_T^2/2R_0 \tag{20.2}$$

where r_0 is the radius of the earth and the other parameters are as defined above.

The height calculated with the above curved-earth algorithm exceeds that calculated by using the flat-earth algorithm, increasing quadratically with measured target range. The discrepancy reaches a value of about 88 ft for a measured target range of 10 nmi.

Spherical Earth: Exact Geometry. Again with reference to Fig. 20.3*b*, the exact target height can be calculated as follows:

$$h_T = [(R_0 + h_a)^2 + R_T^2 + 2(R_0 + h_a)R_T \sin \theta_T]^{1/2} - R_0 \tag{20.3}$$

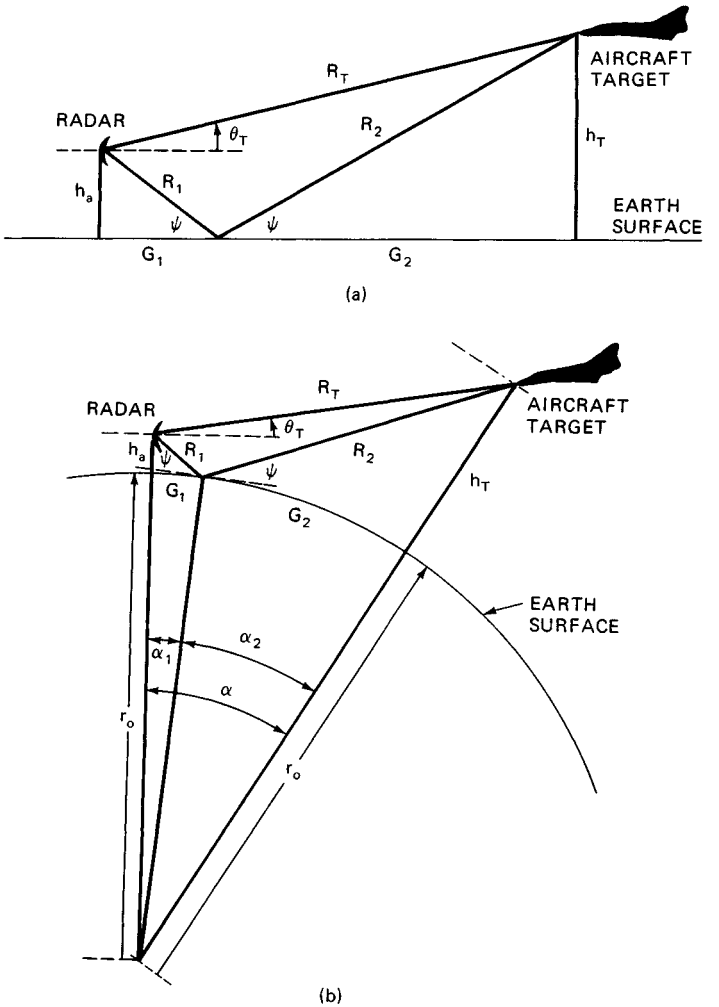

FIG. 20.3 Geometric considerations. (*a*) Flat-earth geometry. (*b*) Spherical-earth geometry.

Corrections for Atmospheric Refraction.* To further improve the accuracy of height computation, refraction of the radar beam along the ray path to the target must be taken into account. In free space, radio waves travel in straight lines. In the earth's atmosphere, however, electromagnetic waves are generally bent or refracted downward. The bending or refracting of radar waves in the atmosphere is caused by the variation with altitude of the index of refraction, which is defined as the ratio of the velocity of propagation in free space to the

*The data tables, figures, and portions of the following discussion on corrections for atmospheric refraction were extracted from and follow closely the original text of Burt Brown's Chap. 22, "Radar Handbook," 1st ed., edited by Merrill Skolnik.[10]

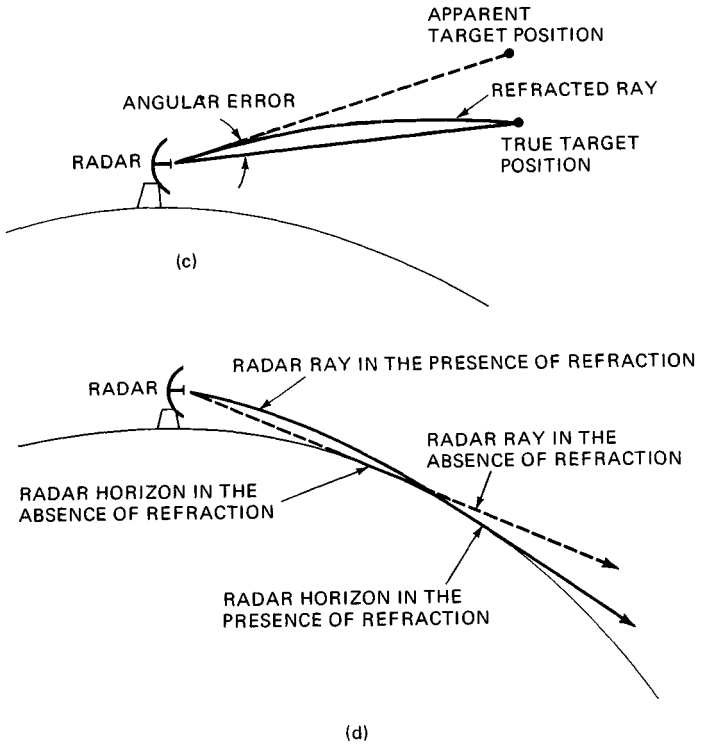

FIG. 20.3 *(Continued)* (*c*) Effect of refraction on radar horizon. (*d*) Angular error due to refraction.

velocity in the medium in question. One effect of refraction is to extend the radar distance to the horizon, as suggested in Fig. 20.3*c*. Another effect is the introduction of errors in the radar measurement of elevation angle. In the tropospheric portion of the atmosphere, the index of refraction n is a function of such meteorological variables as temperature, pressure, and water vapor and can be represented by[30]

$$(n - 1) \times 10^6 = N = \frac{77.6p}{T} + \frac{3.73 \times 10^5 e}{T^2} \tag{20.4}$$

where T = air temperature, K; p = barometric pressure, in millibars; and e = partial pressure of water vapor, in millibars. The parameter N is a scaled index of refraction termed *refractivity*.

Since the barometric pressure p and the water vapor content e decrease rapidly with height, the index of refraction normally decreases with increasing altitude. In a standard atmosphere, the index decreases at a rate of about 4.5×10^{-8} per meter of altitude. A typical value of the index of refraction at the surface

of the earth is of the order of 1.0003. The Cosmic Ray Physics Laboratory (CRPL) standard atmosphere has been defined as one having an index of refraction of 1.000313 (or 313 N units for the refractivity N) and having an exponential decrease of refractive index with altitude.

$$N = N_s \exp(-ah) \tag{20.5}$$

where $N_s = 313$ N units is the surface refractivity and $a = 0.04385$ per kft when h is in thousands of feet.

The classic method of accounting for atmospheric refraction in radar height computations is to replace the actual earth radius R_0 (= 3440 nmi) by an equivalent earth of radius $R_e = kR_0$ and to replace the actual atmosphere by a homogeneous atmosphere in which electromagnetic waves travel in straight lines rather than curved lines (Sec. 2.6). It may be shown by Snell's law in spherical geometry that the value of the factor k by which the earth's radius must be multiplied in order to plot the ray paths as straight lines is

$$k = \frac{1}{1 + R_0 (dn/dh)} \tag{20.6}$$

where dn/dh is the rate of change of refractive index n with height. The vertical gradient of the refractive index dn/dh is normally negative. If, contrary to the CRPL standard atmosphere assumption, it is assumed that this gradient is constant with height, the value of k is 4/3. The use of the 4/3 effective earth's radius to account for the refraction of radio waves has been widely adopted in radio communications, propagation work, and radar.[31] The height calculated by using a 4/3 effective earth's radius is less than that calculated by using the actual earth radius, the difference increasing quadratically with measured target range, attaining a value of about 22 ft at 10 nmi.

The distance d to a horizon from a radar at height h_a may be shown from simple geometry to be approximately

$$d = \sqrt{2kR_0h_a} \tag{20.7}$$

where h_a is assumed to be small compared with R_0. For $k = 4/3$, the above expression reduces to a particularly convenient relationship if d and h_a are measured in nautical miles and feet respectively:

$$d(\text{nmi}) = 1.23\sqrt{h_a(\text{ft})} \tag{20.8}$$

Refined computations of the angular deviations introduced when electromagnetic waves traverse a medium other than free space are discussed elsewhere.[32,33] Estimates of the height error for a target located at an altitude of 100,000 ft based on CRPL Reference Refractivity Atmosphere—1958, are contained in Table 20.1. It is noted that the magnitude of the height error is directly related to the surface refractivity and that above approximately 40° elevation angle the height error is independent of the surface refractivity. The height error is given in Table 20.2 as a function of slant range.

TABLE 20.1 Estimates of Height Error at an Altitude of 100,000 Ft Based on the CRPL Reference Refractivity Atmosphere—1958

Elevation angle,°	Height error, kft		
	Surface refractivity, $N_0 = 280$	Surface refractivity, $N_0 = 315$	Surface refractivity, $N_0 = 370$
1	9.14	11.12	14.73
2	5.65	6.75	8.63
4	2.63	3.08	3.82
6	1.44	1.68	2.06
8	0.89	1.03	1.26
10	0.60	0.69	0.84
15	0.28	0.32	0.39
20	0.16	0.18	0.22
40	0.04	0.04	0.05
70	0.01	0.02	0.02

TABLE 20.2 Estimate of Height Error at Slant Ranges of 100, 200, and 300 nmi Based on the CRPL Reference Refractivity Atmosphere—1958

Elevation angle,°	Height error, kft					
	Slant range, 100 nmi		Slant range, 200 nmi		Slant range, 300 nmi*	
	$N_0 = 280$	$N_0 = 370$	$N_0 = 280$	$N_0 = 370$	$N_0 = 280$	$N_0 = 370$
1	1.61	2.68	5.08	8.07	9.14	14.73
2	1.38	2.32	4.20	6.34		
4	1.12	1.73				
6	0.93	1.36				
8	0.78	1.13				

*Approximate slant range.

TABLE 20.3 Comparison of Heights Based on 4/3-Earth's-Radius Principle with Heights Based on the Exponential Model*

Elevation angle,*	Slant range, 100 nmi			Slant range, 200 nmi			Slant range, 300 nmi		
	h_{exp}	$h_{4/3}$	Δh†	h_{exp}	$h_{4/3}$	Δh	h_{exp}	$h_{4/3}$	Δh
0.0	6.9	6.8	0.1	28.0	26.8	1.2	65.1	60.2	4.9
0.5	12.3	12.1	0.2	39.4	37.4	2.0	82.9	75.9	7.0
1.0	17.8	17.5	0.3	50.6	48.0	2.6			
2.0	28.6	28.1	0.5	72.8	69.1	3.7			
4.0	50.0	49.2	0.8						

*After Bauer, Mason, and Wilson.[34,35]
†$\Delta h = h_{exp} - h_{4/3}$; all heights in kilofeet.

A comparison of the heights based on a 4/3-earth's-radius principle with the heights based upon the exponential model is illustrated in Table 20.3. The data shows that, for a given elevation angle, the difference in height computation increases with slant range and that, for a given range, the height difference increases with elevation angle.

Compensation for Surface Refractivity Variation. For extremely accurate height calculations at long ranges, it is possible to correct for variations in surface refractivity in otherwise normal atmospheric refraction conditions. Such a technique is used, for example, in the General Electric series of solid-state 3D radars. The approach is to use offline ray tracing with an exponential model for atmospheric refraction. The resulting heights are then pretabulated as a function of elevation angle, range, and surface refractivity along with the partial derivatives of the height function with respect to the three above variables. These calculations are then stored in the radar computer database. In normal radar operation, the surface refractivity is measured periodically at the radar site, where it is used in conjunction with measured target elevation θ_T and range R_T to perform online table lookup of the tabulated height-refractivity parameters. The final height is computed by means of the interpolation

$$h_T = h_T(R_k,\theta_k,N_k) + \frac{\partial h_T}{\partial R_k}(R_T - R_k) + \frac{\partial h_T}{\partial \theta_k}(\theta_T - \theta_k) + \frac{\partial h_T}{\partial N_k}(N - N_k) \tag{20.9}$$

where R_k, θ_k, and N_k are the closest stored values of range, elevation angle, and surface refractivity to the measured values.

Practical Corrections

Terrain Height Adjustments. If the height of the target above local terrain is to be obtained, the height relative to mean sea level must be corrected by the height of the terrain below the target. This involves calculation of ground range from target slant range and elevation angle and computer lookup of terrain height versus ground range and azimuth.

Platform Location, Orientation, and Stabilization. The calculation of target height with a radar on a moving platform, such as a ship, aircraft, or satellite (all of which are subject to uncertainties in location and orientation) is somewhat more complicated. Coordinate conversion of measured target range, azimuth, and elevation is necessary to determine the target height. Platform location and orientation must be sensed, and perhaps stabilized, and provided to the radar computer. Some of these quantities are also required for platform navigation and therefore may be available from the navigation gyros.

20.3 HEIGHT ACCURACY PERFORMANCE LIMITATIONS

The accuracy of the measurement of target height with a radar is conveniently expressed in terms of the root-mean-square error (rmse), i.e., the square root of the expected value of the square of the difference between the estimated target height and the actual target height. Because height is a derived quantity from the basic radar measurements of range and elevation angle, height accuracy can be expressed in terms of the rms errors associated with those measurements, as suggested in Table 20.4. The remainder of this section is devoted to analysis of the errors involved in the basic radar measurements, primarily elevation angle.

All radar measurements are in error because of the contamination of the received-signal echo with thermal noise. The common assumption about the nature of thermal noise, well justified by practical experience, is that it is a narrowband zero-mean gaussian random process. A particular pair of samples consisting of in-phase (I) and quadrature (Q) components can be properly

TABLE 20.4 Relationship of Target Height Error to Radar Range and Elevation Angle Measurement Errors*

Flat earth:

$$\sigma_h = (\sigma_R^2 \sin^2\theta + R^2\sigma_\theta^2 \cos^2\theta)^{1/2}$$

Spherical earth: parabolic approximation:

$$\sigma_h = [\sigma_R^2(R/R_e + \sin\theta)^2 + R^2\sigma_\theta^2 \cos^2\theta]^{1/2}$$

Spherical earth: exact geometry:

$$\sigma_h = \{[\sigma_R^2(R^2 + (R_e + h_a)^2 \sin^2\theta) + (R_e + h_a)^2R^2\sigma_\theta^2 \cos^2\theta]/(R_e + h)^2\}^{1/2}$$

R_e = effective earth radius = kR_0
h_a = antenna height above earth surface
R = radar-measured target range
θ = radar-measured target elevation angle
h = radar-measured target height
σ_R = rmse of radar range measurement
σ_θ = rmse of radar elevation-angle measurement
σ_h = rmse of target height estimate

*Colocated and exactly known platform-antenna location and orientation and small measurement errors relative to target coordinate values are assumed.

viewed, therefore, as a single complex zero-mean gaussian random variable.* The rmse associated with the accuracy performance of a particular radar angle measurement technique, as limited solely by the presence of thermal noise on the technique, is termed herein the *fundamental accuracy* of the technique.

The fundamental accuracy of two general categories of elevation-angle estimation techniques is presented in this section: the sequential-lobing technique and the simultaneous-lobing technique. Other practical effects influencing the height accuracy of a radar system include: beam-pointing errors, pattern errors, channel mismatch errors, calibration, platform orientation and gyration, stabilization, compensation, ECM-ECCM and clutter errors, multipath, target fluctuations and thresholding effects, and multiple hit and channel combining.

Fundamental Accuracy of Sequential Lobing. Sequential lobing is a technique used in radar for estimating the angle of arrival of electromagnatic radiation incident on an antenna by comparing the amplitudes of the received echoes in two or more sequentially formed or selected antenna beams. The technique is used for height finding by time—sequentially scanning a beam in elevation while transmitting and receiving pulses in each beam position. The pulse amplitudes in each beam position are envelope-detected and stored for use in a comparison with those from the other beams. The simplest form of radar sequential lobing compares the envelope-detected returns from a single pulse in each of two adjacent beams. The ratio of the detected pulse amplitude in one beam position to that in the other forms the basis for a table lookup or readout of target elevation angle. In early radar the readout was a calibrated dial or display. In 3D radars, computers provide elaborate lookup tables to relate the ratios to the target elevation angle.

The envelope-detected target returns in each of the beam positions are corrupted by thermal noise even in the most ideal of circumstances. This noise is due

*The term *complex* here refers to $I + jQ$. The complex sample has zero mean because of its random uniformly distributed phase on the interval $(0,2\pi)$.

to thermally generated electronic noise in the radar receivers and to noiselike electromagnetic emissions from the sky and ground entering the antenna.

For a nonfluctuating target, a good approximation for the fundamental accuracy of the sequential-lobing technique for a large signal-to-noise ratio* is

$$\text{rmse} = \frac{1}{|\dot{f}|}\left(\frac{1 + f^2}{2x}\right)^{1/2} \tag{20.10}$$

where, if θ is the target angle and $\hat{\theta}$ is its estimate, the rmse is defined by $[E(\hat{\theta} - \theta)^2]^{1/2}$. The various factors in the above rmse are defined as

$f = f(\theta) = G_2(\theta)/G_1(\theta)$ = ratio of two-way elevation beam power patterns
$\dot{f} = df/d\theta$; gives rmse in radians or milliradians (mrad)
$\dot{f} = df/d\,(\sin\theta)$; gives rmse in sines or millisines (msine)
$G_2(\theta)$ = two-way elevation beam power pattern in beam position 2
$G_1(\theta)$ = two-way elevation beam power pattern in beam position 1
x = signal-to-noise ratio in beam position 1

Note that this result may be put into the familiar form

$$\text{rmse} = \frac{1}{K\sqrt{2x_0}} \tag{20.11}$$

$$\text{where } K = \frac{|\dot{f}|\,|g_1|}{(1 + f^2)^{1/2}} \tag{20.12}$$

g_1 = two-way normalized voltage pattern in beam position 1
$= G_1^{1/2}/G_{10}^{1/2}$; G_{10} = boresight antenna power gain in beam 1
and, x_0 = boresight signal-to-noise ratio

The constant K in this form is a measure of the sensitivity of the angle estimation technique, in that the larger K is, the smaller are the rms errors and the better is the angle accuracy. A single value of the sensitivity (at beam peak or at crossover) is often used to compare techniques. However, care must be taken in this practice, because K is a strong function of the antenna beamwidth and of the target angle of arrival relative to the position of the beams in angle space. As expressed above, K includes the signal-to-noise-ratio dependence on the target angle through the two-way pattern of the beam. An alternative formulation could leave this pattern factor in the signal-to-noise ratio and omit it from the definition of K.

The fundamental accuracy of the sequential-lobing technique for a scanning beam generated by a uniformly illuminated aperture on transmit and receive is presented in Fig. 20.4*a*. Performance is presented in terms of a normalized ver-

*The signal-to-noise-ratio definition used here is E/N_0, where E is the received pulse energy and $N_0/2$ is the spectral power density of the interfering thermal noise.

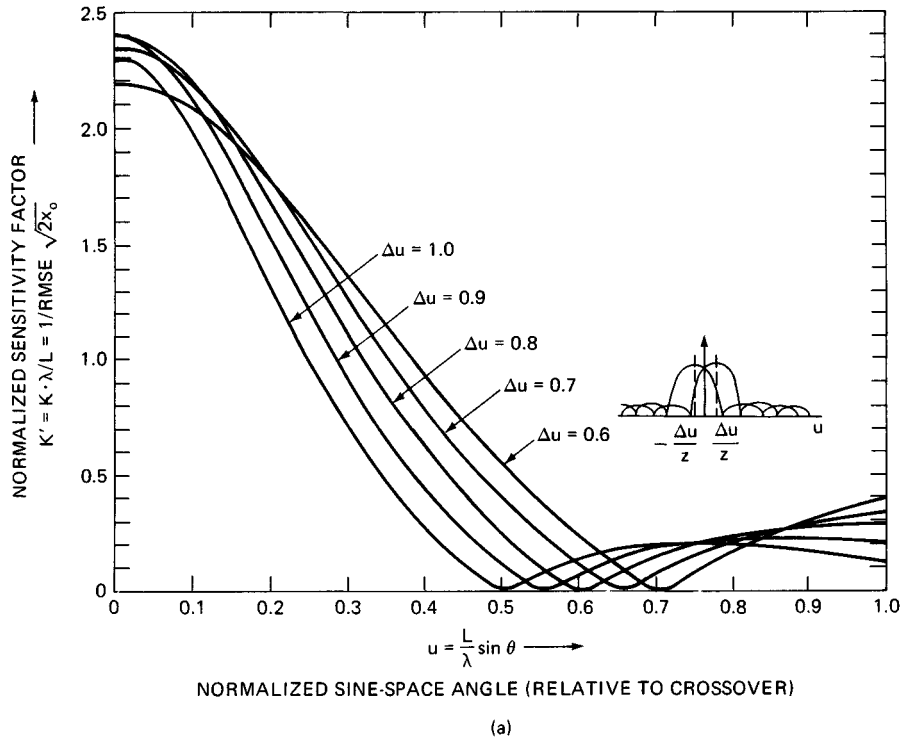

FIG. 20.4 Fundamental accuracy. (*a*) Two-beam sequential lobing: uniform (sin $\pi u/\pi u$) sum beams transmit and receive; separation = Δu; nonfluctuating target; N = one pulse per beam.

sion of the sensitivity factor $k = K\lambda/L$ versus a similarly normalized sine-space elevation angle of arrival, $u = L/\lambda \sin(\theta)$. The elevation angle θ is referenced to the crossover point halfway between the beam peaks. This normalization removes the aperture dimension L and transmit wavelength λ from the performance of the technique. The figure shows that the sensitivity factor peaks at crossover and is symmetrical about the crossover angle. The value of the normalized sensitivity factor at crossover depends on the two-way beam shape–aperture illumination and the step size between the beams. For a uniformly illuminated aperture whose beam is stepped by $\Delta u = 1$, between single-pulse transmission/reception, the normalized sensitivity factor associated with the two-beam sequential-lobing technique against a nonfluctuating target attains a value of approximately 2.15 at the crossover angle. Thus, for example, if the aperture height is 24 ft (7.3 m) and the radar is L band ($\lambda = 0.23$m), the appropriate normalization factor is $L/\lambda = 31.75$, so that the actual sequential-lobing sensitivity factor for a target at crossover is 68.25 V/(V · sine*), or 0.06825 V/(V · msine*). If the boresight

*A *sine* or a *millisine* is a unit of measure of the sine of an angle. For example, an angle of 0.7 rad (700 mrad) corresponds to sin (0.7) 0.64422 sine = 644.22 msines.

signal-to-noise ratio is 100 (20 dB), the rmse is easily calculated as rmse = 1.04 msines. Furthermore, if the beams have been electronically steered so that their crossover elevation angle is, say, 30° away from the antenna broadside, the angular accuracy can be calculated as rmse = 1.04/cos (30°) = 1.2 mrad.

If the beams are too closely spaced, sensitivity suffers because there isn't sufficient difference in the received echo strength to measure the angle of arrival accurately. On the other hand, if they are separated too far, there isn't sufficient signal-to-noise ratio in one of the beams for accuracy. It follows that there is a beam step size that optimizes accuracy by maximizing sensitivity and minimizing errors. This is clearly illustrated in Fig. 20.4*a*, which shows a maximization of the sensitivity factor for a beam spacing between $\Delta u = 0.8$ and $\Delta u = 0.9$. It can be shown analytically (for gaussian beam shapes) that the optimum spacing between beams is $\Delta u = 0.85$. It is also significant to note that the valid range of angular (u-space) coverage for the sequential-lobing technique using uniform illuminated sum beams is approximately $2 - \Delta u$, where Δu is the beam step size between transmission in u space. Within this region, the target is in the main lobe of each of the two beams, and its angle is uniquely and unambiguously determined by the ratio of the echo strengths in the two beams. Outside this region the target is in the sidelobes of at least one of the beams, and its angle of incidence cannot be unambiguously estimated with the technique. In practice, sidelobe responses to a target are eliminated by the use of sidelobe blanking. At the optimum beam spacing of $\Delta u = 0.85$, the valid angular coverage is $2 - 0.85 = 1.15$, or ± 0.575 about the crossover angle. Coverage can be increased from this value by decreased step size or by aperture weighting, but only at the expense of sensitivity.

It is possible to utilize more than two beam positions in the sequential-lobing estimation algorithm. In such an approach, performance is improved when the beam scans a small amount in angle between transmissions. As the beam steps past the target in elevation, it is possible to display intensity, or target echo strength, on a display or other indicator at the angular locations of the beam. A centroidal interpolation of the angular locations as weighted by the receive pulse amplitudes may be used to extract the target angle estimate. The mathematically equivalent estimation process is

$$\hat{\theta} = f^{-1}\left(\frac{\sum_{k=1}^{N} |r_k| \theta_k}{\sum_{k=1}^{N} |r_k|}\right) \tag{20.13}$$

where r_k = complex $(I_k + jQ_k)$ sample at receiver–pulse matched-fiber output
θ_k = boresight elevation of beam position k
N = number of beam positions used in algorithm

and $$f(\theta) = \sum_{k=1}^{N} \theta_k g_k \Big/ \sum_{k=1}^{N} g_k \qquad g_k = g_k(\theta) = G_k^{1/2}(\theta)/G_0^{1/2}$$

where G_0 = boresight gain of beam. The fundamental accuracy of this multiple-beam position version of the sequential-lobing estimation algorithm is

$$\text{rmse} = \left[\frac{\sum_{k=1}^{N} (\theta_k - f)^2}{2\dot{f}^2 x_0 \left(\sum_{k=1}^{N} g_k \right)^2} \right]^{1/2} \tag{20.14}$$

This performance can be calculated at an arbitrary elevation angle between the beams θ, or it can be averaged over an elevation angle in a root-sum-square (rss) sense as

$$\overline{\text{rmse}} = \left(\frac{1}{\theta_s} \int_0^{\theta_s} \text{mse}(\theta)\, d\,\theta \right)^{1/2} \tag{20.15}$$

where θ_s is the angular separation between the beam positions and mse(θ) is the mean square error.

Figure 20.4*b* displays this rss average accuracy for a nonfluctuating target versus signal-to-noise ratio for various beam spacings of a gaussian-shaped scanning beam. In general, the fundamental accuracy performance of the sequential-lobing technique is a function of the beam shapes and separations, the number of pulses

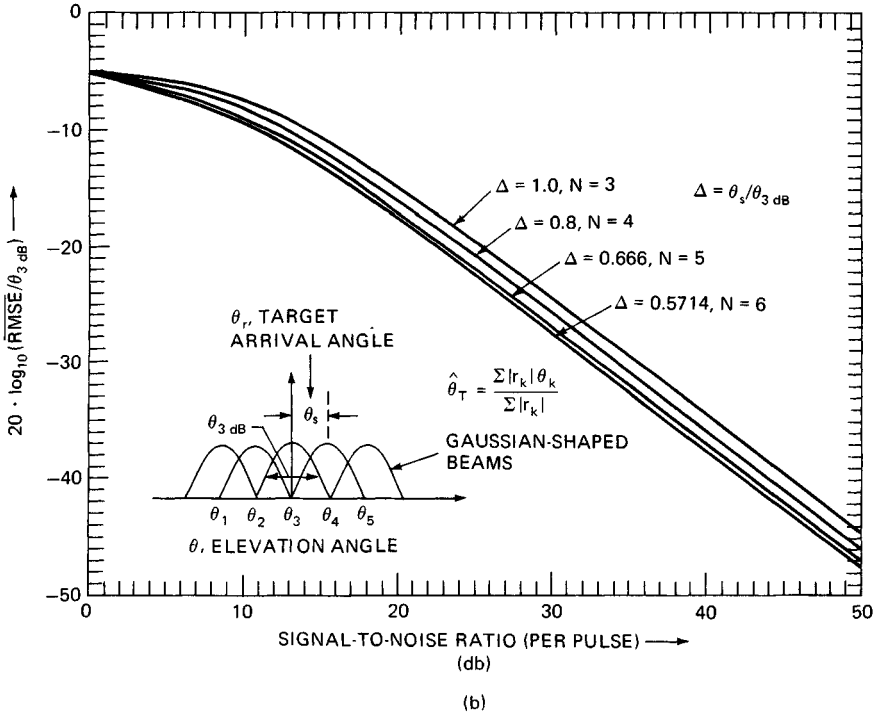

(b)

FIG. 20.4 *(Continued)* Fundamental accuracy. (*b*) Multiple-beam sequential lobing: nonfluctuating target.

noncoherently integrated in each beam, the type and amount of target echo pulse-to-pulse fluctuation within a beam, and of the prevailing beam-to-beam correlation in target fluctuation. For N pulse returns noncoherently integrated within each beam on a nonfluctuating target, the asymptotic rmse accuracy performance of two-beam sequential lobing is given by

$$\text{rmse} = \left(\frac{1 + f^2}{2f^2 Nx}\right)^{1/2} \tag{20.16}$$

where f = ratio of two-way elevation power patterns as before
N = number of pulses noncoherently integrated
x = per-pulse SNR

Since this form is the same as for a single pulse except for the factor of N in the denominator, numerical results may be obtained from Fig. 20.4*a* with appropriate scaling.

Fundamental Accuracy of Simultaneous Lobing. In the simultaneous-lobing method of angle estimation, two or more radar receive beams are simultaneously formed by the antenna and processed in parallel receive channels. A single transmit beam covers the angular region to be simultaneously processed on receive. Stacked beams, monopulse, and phase interferometry are all examples of the use of simultaneous lobing for target elevation angle estimation. While very different in implementation for a radar system, the fundamental accuracies of these techniques are all analyzed in a similar fashion, with approximate results that can be placed in the same form as Eq. (20.11). Because the receive beams in this technique are formed and processed simultaneously, the relative phase of the return between receive channels can, if desired, be used to aid the angle extraction accuracy. If it is used, the process is termed *phase-coherent* or simply *coherent*, and a close match in phase between receive channels must be maintained.

Monopulse. In general, the term *monopulse* refers to a radar technique to estimate the angle of arrival of a target echo resulting from a single-pulse transmission by using the amplitude and/or phase samples of the echo in a pair of simultaneously formed receive beams (Sec. 18.3). Historically the term has been associated with the simultaneous generation and processing of a *sum* receive beam and a *difference*, or *delta*, receive beam. These beams are so named because of the early and still common method used to form them, i.e., by adding and subtracting, respectively, the two halves of the antenna aperture. While this method is a relatively inexpensive way to produce a sum-difference beam pair, it is not necessarily the best way from a performance standpoint. Furthermore, it is unnecessarily constraining in many phased array applications, especially where the feeds account for a small fraction of the cost of the total radar. Typically a sum beam may be designed for good detectability and sidelobes. The delta beam is then optimized for accuracy performance, perhaps with other constraints. The defining characteristic of a sum beam is that it has approximately even symmetry about the beam boresight, while a delta beam has approximately odd symmetry about the same boresight. Without loss of generality, the delta beam may be assumed to be adjusted or calibrated to be in phase with the sum beam, in the sense that the ratio of the two patterns is real and odd about the beam boresight versus angle of arrival.

Monopulse techniques are classified according to the manner in which the incident radiation is sensed, i.e., according to antenna and beamforming techniques, and independently according to how the various beams and channels are subsequently processed and combined to produce a target angle estimate.[36,37] Amplitude comparison monopulse and phase comparison monopulse are categories of antenna-beamforming *sensing* techniques. In amplitude comparison monopulse, the antenna-beamformer generates a pair of sum and difference beams which, without loss of generality, may be assumed to be in phase, in the sense that their ratio is real. In phase comparison monopulse, two or more antennas or sets of radiating-receiving elements, physically separated in the elevation dimension, are used to generate two beams which have ideally identical patterns except for a phase difference which depends on the angle of incidence of the received target echo. Each of these techniques may be converted to the other, either in concept through mathematical sums and differences or physically through the use of passive RF hybrid combining devices. The fundamental accuracy performance of a phase comparison monopulse system is identical to that of an amplitude comparison monopulse system converted by this method, and vice versa. Therefore, the fundamental accuracy performance is addressed here from the conceptual viewpoint of amplitude comparison monopulse.

There are a variety of ways to implement monopulse processing on a sum-difference beam pair, depicted functionally in Fig. 20.5, some of which have a substantial impact on the fundamental monopulse accuracy performance. In each of these implementations, returns from a single transmission are received in simultaneously formed sum and difference beams and processed coherently. In the full-vector monopulse of Fig. 20.5*a*, two complex (*I*, *Q*) samples are fully utilized to calculate a complex monopulse ratio statistic. This calculated statistic, the *measured* monopulse ratio, provides the basis for a computer table lookup of the target angle of arrival relative to the null in the delta beam. The computer lookup function is simply a tabulated version of the assumed monopulse ratio consisting of the assumed delta beam antenna pattern to that of the assumed sum beam versus angle off-beam boresight. The tabulated monopulse ratio is inverted in the lookup process by entering the table with the measured monopulse ratio and finding the corresponding off-boresight angle. The full-vector monopulse processing in Fig. 20.5*b* differs somewhat from that in Fig. 20.5*a*, in that after low-noise amplification to establish the system noise figure, an RF quadrature hybrid device is used to combine the delta and sum beam signals 90° out of phase, i.e., as $\Sigma + j\Delta$. The purpose of this combining in the difference channel is to bring the signal strength in the difference channel to approximately the same amplitude at that in the sum channel. This causes unavoidable receiver nonlinearities to have nearly the same effect in the two channels, resulting in less degradation in accuracy performance attributable to receive-string nonlinearities. In the absence of nonlinearities, the two techniques in Fig. 20.5*a* and *b* are mathematically identical because

$$\mathrm{Im}\left(\frac{\Sigma + \mathrm{j}\Delta}{\Sigma}\right) = \mathrm{Im}\left(1 + \mathrm{j}\frac{\Delta}{\Sigma}\right) = \mathrm{Im}\left|\frac{\Delta}{\Sigma}\right| \cos\phi \tag{20.17}$$

Hence, they both provide the fundamental accuracy performance of full-vector monopulse processing, given by

$$\mathrm{rmse} = \frac{\|w_\Delta - f w_\Sigma\|}{|\dot{f}|(2x)^{1/2}} \tag{20.18}$$

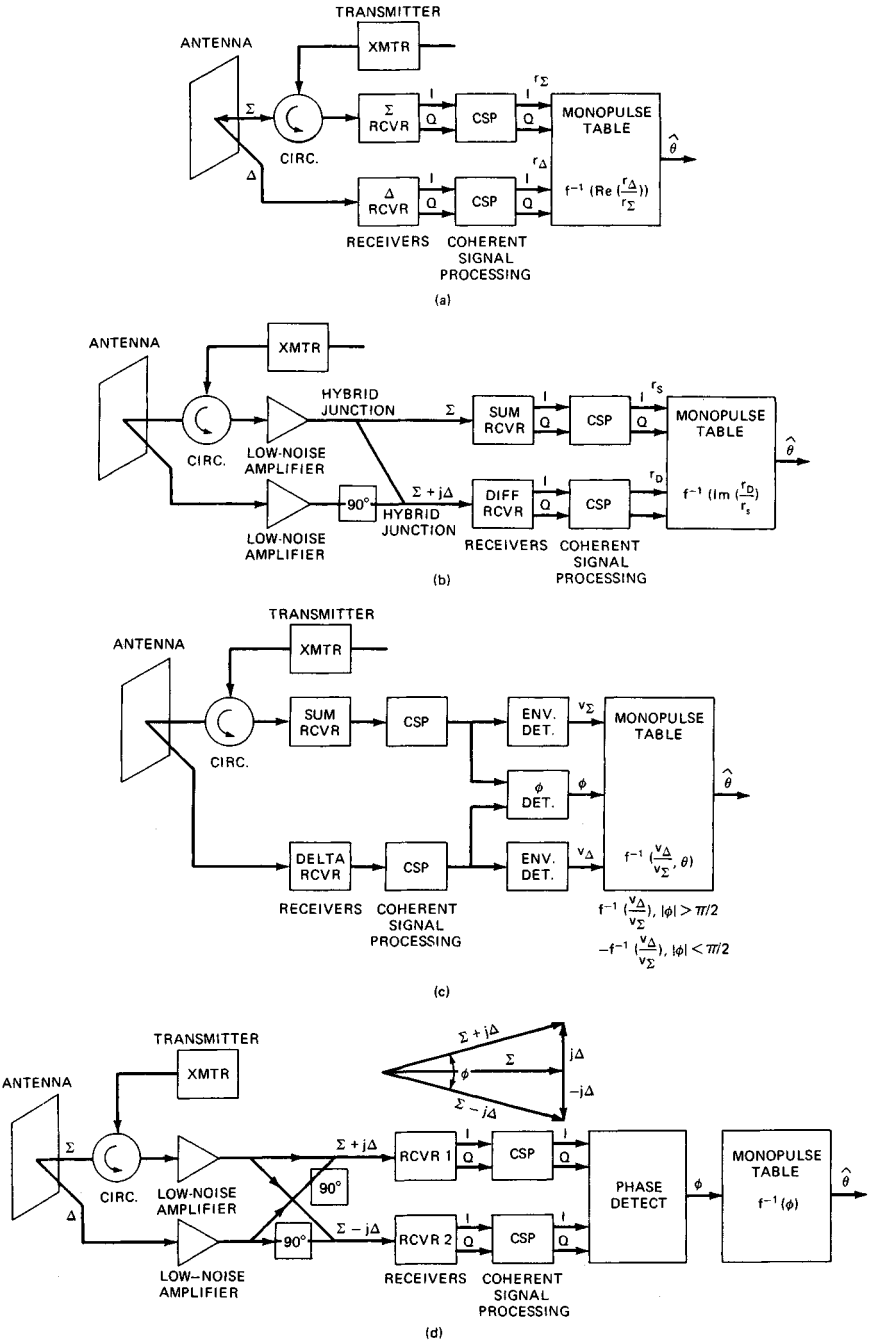

FIG. 20.5 Functional monopulse processing implementations. (*a*) Full-vector monopulse processing. (*b*) Full-vector monopulse with prehybrid combining. (*c*) Amplitude-only monopulse processing. (*d*) Phase-only monopulse processing.

where $f = f(\theta) = \Delta(\theta)/\Sigma(\theta)$, x = signal-to-noise ratio in the sum beam, and

Continuous aperture	*Discrete aperture array*
$w_\Delta = w_\Delta(x)$ aperture illumination	$w_\Delta = (w_{\Delta n})$ $n=1, N$ vectors of
$w_\Sigma = w_\Sigma(x)$ functions	$w_\Sigma = (w_{\Sigma n})$ array weights
$\|\|w_\Delta\|\| = \left(\int_{-\infty}^{\infty} \|w_\Delta(x)\|^2 dx\right)^{1/2}$	$\|\|w_\Delta\|\| = \left(\sum_1^N \|w_{\Delta n}\|^2\right)^{1/2}$
$\|\|w_\Sigma\|\| = \left(\int_{-\infty}^{\infty} \|w_\Sigma(x)\|^2 dx\right)^{1/2}$	$\|\|w_\Sigma\|\| = \left(\sum_1^N \|w_{\Sigma n}\|^2\right)^{1/2}$
$\Delta(\theta) = \int_{-\infty}^{\infty} w_\Delta(x) \exp(j2\pi x(\sin\theta))dx / \|\|w_\Delta\|\|$	$\Delta(\theta) = \sum_1^N w_{\Delta n} \exp[j2\pi x_n(\sin\theta)] / \|\|w_\Delta\|\|$
$\Sigma(\theta) = \int_{-\infty}^{\infty} w_\Sigma(x) \exp(j2\pi x(\sin\theta)dx / \|\|w_\Sigma\|\|$	$\Sigma(\theta) = \sum_1^N w_{\Sigma n} \exp[j2\pi x_n(\sin\theta)] / \|\|w_\Sigma\|\|$

Various authors have defined the *monopulse sensitivity factor* in different ways.[38] For the purposes of this chapter, the monopulse sensitivity factor is defined as the constant of proportionality required in the denominator of the rmse to convert the square root of twice the boresight signal-to-noise ratio in the beam to the rmse. Defined in this manner, the monopulse sensitivity factor has the desirable property of containing all target elevation angle-of-arrival information.

The monopulse sensitivity factor for full-vector monopulse is

$$K = \frac{|\dot{f}|\,|g_\Sigma|\,|g_T|}{\|w_0 - f w_\Sigma\|} \tag{20.19}$$

where $g_\Sigma = g_\Sigma(\theta) = \Sigma(\theta)/\Sigma_0$ = sum-beam voltage pattern normalized to unity gain

$g_T = g_T(\theta) = G_T(\theta)/G_{T0}$ = transmit-beam voltage pattern normalized to unity gain

For orthogonal aperture illumination functions, where $\Sigma_{k=1}^N w_{\Sigma k} w^*_{\Delta k} = 0$ (usually the case in practice), this equation reduces to

$$K = \frac{|\dot{f}|\,|g_\Sigma|\,|g_T|}{(1 + f^2)^{1/2}} \tag{20.20}$$

This performance is presented graphically for several cases of interest in Fig. 20.6. A normalized sensitivity factor $k = K\lambda/L$ is plotted versus the u-space elevation angle of arrival $u = L/\lambda \sin\theta$, with θ referenced to the boresight of the sum and delta beams. The monopulse sensitivity factor peaks and is symmetrical about the boresight angle. The two curves in Fig. 20.6*a* correspond to uniformly illuminated sum beams. In one case, the delta beam is formed by subtracting the upper and lower halves of a uniformly illuminated aperture. For this delta beam illumination function, the normalized boresight monopulse sensitivity is $\pi/2 \approx 1.57$. The sensitivity degrades off boresight, despite an increasing monopulse ratio slope, owing to a decreasing signal-to-noise ratio in the two channels and to

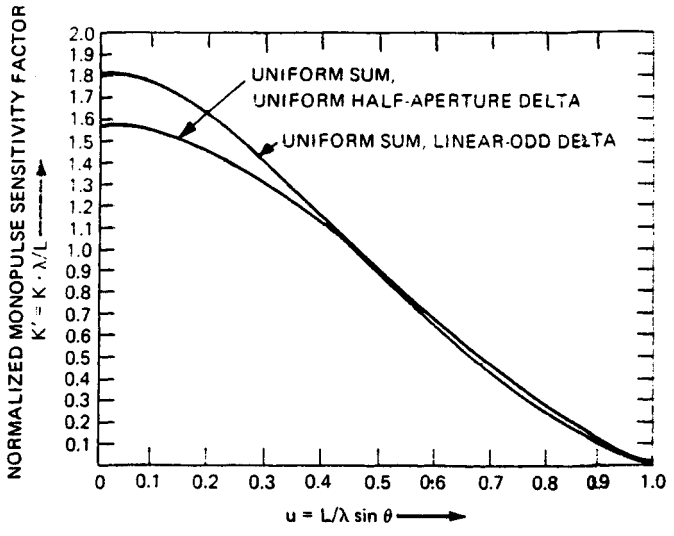

(a)

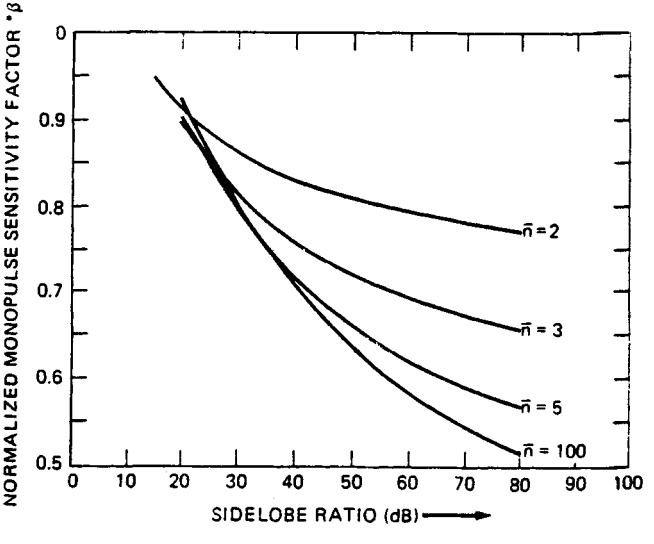

$*\beta = \frac{RMSE_0}{RMSE}$; = accuracy with Taylor Σ, Bayliss Δ; $RMSE_0$ = accuracy with uniform Σ, linear-odd Δ.

(b)

FIG. 20.6 Fundamental accuracy of monopulse. (*a*) Vector monopulse accuracy: two common monopulse aperture illumination pairs. (*b*) Boresight vector monopulse sensitivities of Taylor sum and Bayliss delta aperture illuminations.

an increasing absolute value of the monopulse ratio $f(\theta)$. It can be shown that the boresight sensitivity of full-vector monopulse with a uniform sum beam can be maximized at a value of approximately 1.8 by employing a linear-odd aperture illumination function to generate the delta beam. The second curve in Fig. 20.6*a* illustrates performance for a linear-odd delta beam aperture illumination. The actual monopulse sensitivity factor can be calculated from the normalized sensitivity once the aperture height and RF wavelength have been specified. As an example, if $L/\lambda = 31.75$, the boresight monopulse sensitivity factor corresponding to the linear-odd delta beam illumination function is 0.05715 V/(V·msine). With a 20 dB signal-to-noise-ratio target return, this corresponds to a fundamental accuracy of 1.24 msines. For a uniform beam, the range of valid u-space angle coverage is approximately 2.0, corresponding to the sum-beam main-lobe null-to-null width. This is a principal advantage of monopulse because it allows reasonable spacings of the monopulse beams for coverage of large surveillance volumes. Coverage is increased with aperture weighting at the expense of monopulse sensitivity and fundamental accuracy. The effect on the boresight monopulse sensitivity of Taylor aperture weighting for the sum beam and Bayliss aperture weighting for the delta beam is illustrated in Fig. 20.6*b*. The sensitivity presented there is normalized by the sensitivity of the uniform-sum, linear-odd delta case, and is plotted for various values of the two parameters used to specify Taylor and Bayliss weighting, $\bar{n}$, and sidelobe ratio (*SLR*). It should be noted that not all combinations of $\bar{n}$ and *SLR* depicted in the figure constitute good aperture illumination design choices.

It is sometimes convenient and/or economical to perform coherent signal processing at RF or IF, by analog techniques, and then to carry out envelope and phase detection in the two channels. In amplitude-only monopulse the purpose of phase detection is solely to tell on which half of the beam the target return is incident. The angle off boresight is then determined via table lookup of the ratio of the envelope-detected signal strengths. The primary disadvantage of this approach is a degradation of accuracy at and near boresight relative to full-vector monopulse. It also provides less flexibility in coherent signal processing since it is analog instead of digital.

The fundamental accuracy performance of amplitude-only monopulse processing is degraded at boresight by the probability of incorrect phase detection, i.e., the probability of deciding that the target is below boresight when it is actually above, or vice versa. This probability is 0.5 at beam boresight, which results in boresight fundamental accuracy which is a factor of 2 worse than that of full vector monopulse. At off-boresight angles, the phase detection error probability depends on the signal-to-noise ratio. At angles far from the beam boresight, the signal-to-noise ratio diminishes, causing the error probability again to approach 0.5. A minimum-error probability–maximum-accuracy condition is reached for intermediate angles.

The last monopulse implementation illustrated (Fig. 20.5*d*) is termed *phase-only monopulse*. This processing is to be distinguished from the technique of phase interferometry, which has also been called by some authors[36,37] *phase-comparison monopulse*. In Fig. 20.5*d*, RF or IF hybrids are used to combine the sum and delta channels in quadrature, i.e., with a 90° phase shift. An accurate phase detector then detects the phase difference between the two channels. The underlying principle is that this phase difference will be in one-to-one correspondence with the delta-to-sum ratio, as illustrated in the vector diagram accompanying Fig. 20.5*d*. In phase-only monopulse, off-boresight accuracy is sacrificed to

gain the benefit of identical amplitude signals in the two receiver-processor channels. If desired, the signals in the two channels may be hard-limited without affecting the fundamental accuracy of the phase-only monopulse processing. In principle, phase-only monopulse can be used to alleviate stringent receiver-processor dynamic-range requirements. However, other aspects of performance may suffer and should be examined carefully in the tradeoff process. Another advantage of phase-only monopulse, relative to vector and amplitude-only, is that the need for precise amplitude matching channel to channel is reduced.

Phase-only monopulse processing does not utilize the full target angle-of-arrival information available in the two beams. For this reason, its fundamental accuracy performance suffers. The fundamental accuracy of phase-only monopulse is identical to that of vector monopulse at boresight but degrades more rapidly off boresight. Full vector monopulse, using all the available information in the target returns, shows superior sensitivity at all target incidence angles. A uniformly illuminated aperture and beam and a uniform half-aperture difference beam are used for comparison of the three implementations.

In a radar which employs vector monopulse processing for height finding, it is possible to coherently precombine the returns from multiple pulses or subpulses in the simultaneous beams to form a single estimate of the target elevation angle of arrival, as suggested in Fig. 20.7. In this approach, the returns in the delta and sum channels are coherently cross-correlated pulse to pulse, and then the real part of the cross-correlation sum is normalized by a term determined by noncoherent integration in the sum channel to form the measured monopulse ratio. The same noncoherent sum used to normalize the measured monopulse ratio may be also used in the target decision logic for detection thresholding.

The rmse for multiple-pulse coherent monopulse differs from that of a single-pulse monopulse only by the square root of the number of pulses in the denominator. The results of Fig. 20.6, appropriately scaled, are applicable.

Stacked Beams. Stacked beams are another example of simultaneous lobing for target elevation-angle estimation. The processing of a pair of beams in the stack consists of an amplitude comparison table lookup. Its fundamental accuracy can also be placed in the form of Eq. (20.11).

In the stacked-beam radar, the transmit beam must be designed to cover all the beams within the stack and is therefore relatively wide in elevation beamwidth compared with that of a receive beam in the stack. A good approximation is that it is isotropic in elevation and thus is not a factor in the fundamental accuracy performance.

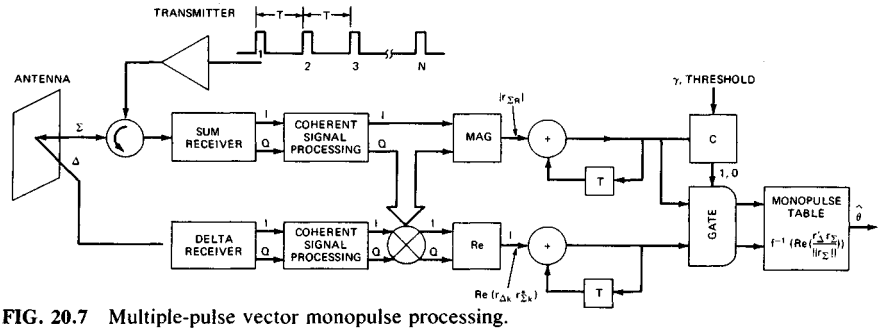

FIG. 20.7 Multiple-pulse vector monopulse processing.

The fundamental accuracy performance of a pair of uniformly illuminated beams in a stack is presented in Fig. 20.8 in terms of a normalized sensitivity factor $k = K\lambda/L$ versus normalized sine-space angle-of-arrival $u = L/\lambda \sin \theta$. The elevation u-space angle of arrival u of target energy is referenced to the crossover point halfway between the beams. Various beam separations in u space are illustrated. The sensitivity of the technique peaks at the crossover angle and is symmetrical about that angle, attaining a value at crossover which depends on the separation between the beams. A maximum crossover sensitivity of 1.95 is achieved for a u-space beam separation of 1.2. Coverage in u space provided by the uniform stacked-beam pair is approximately given by $2-\Delta u$, where Δu is the u-space beam separation corresponding to a target in the main lobes of both beams. Outside this region, the target is in the sidelobes of one of the beams. In a stacked-beam radar, detections are made in a special cosecant-squared type of surveillance beam; so this condition is not sensed in the detection process. Thus, in order to eliminate the possibility of ambiguities, uniformly illuminated beams should be stacked at $\Delta u \leq 1$. The coverage of each beam pair may be increased by aperture weighting. In this case the beams may be stacked at greater separations but will possess reduced crossover sensitivity. The normalized crossover sensitivity associated with a pair of uniformly illuminated sum beams spaced at $\Delta u = 1$ is approximately 1.8. This corresponds to a fundamental accuracy of approximately 1.24 msines for a 24-ft aperture height at L band with a 20 dB target boresight signal-to-noise ratio.

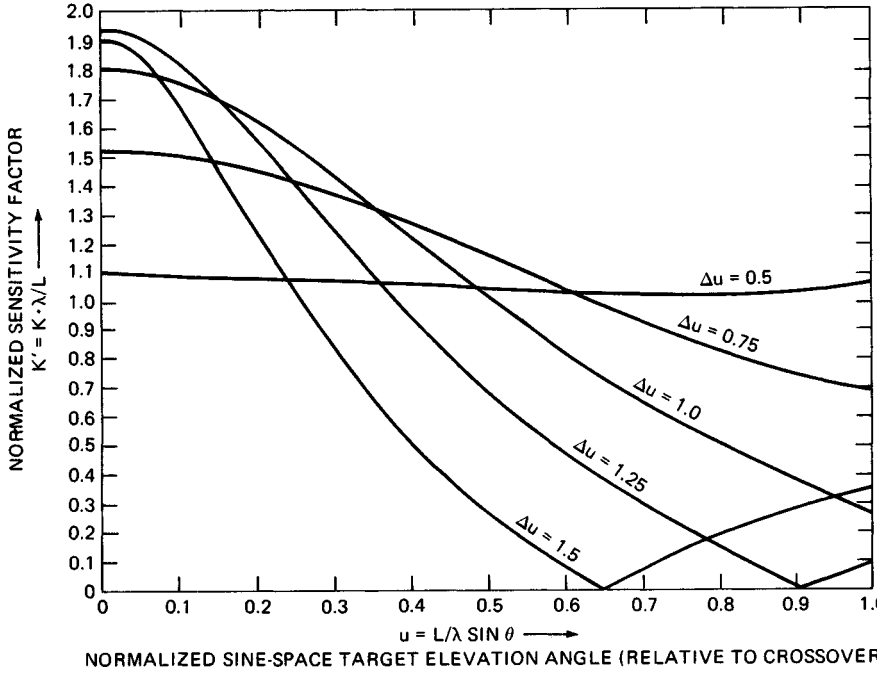

FIG. 20.8 Fundamental accuracy of stacked beams.

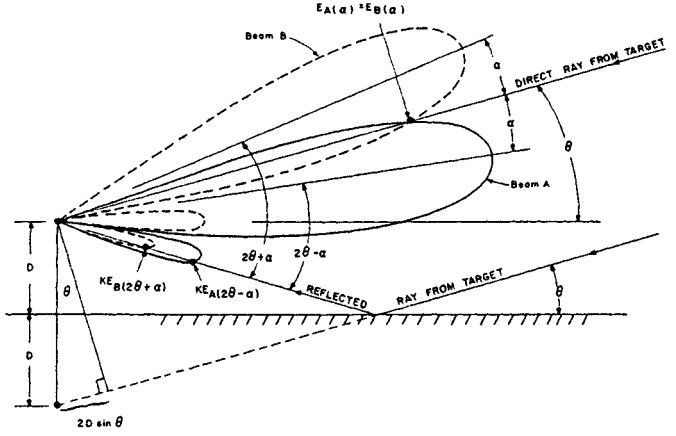

FIG. 20.9 Geometry for the analysis of elevation errors due to ground reflections in a simultaneous amplitude comparison radar.

Elevation Error Due to Surface Reflections.* One of the fundamental factors limiting the height accuracy in all height finding techniques that depend on elevation-angle measurements is the elevation-angle accuracy degradation due to the multipath from surface reflections. Such surface reflections vectorially combine with the direct-path signals entering the antenna to produce amplitude and phase variations which ordinarily cannot be separated from the direct-path signals. In general, the magnitude of such elevation-angle errors is such that, at low elevation angles where an appreciable portion of the antenna beam is directed into the ground, the elevation-angle errors are prohibitively large. Therefore, as a general rule, pencil-beam height finding radars and elevation-tracking radars cannot be expected to produce reliable elevation-angle data when their beams are pointed within about one beamwidth (−3 dB beamwidth) above the ground. At larger elevation angles, the magnitude of the elevation errors is a direct function of the ground-reflected relative field strength received in the respective negative-angle elevation sidelobe (i.e., the product of the relative sidelobe level and the ground-reflection coefficient).

Radar systems that employ a simultaneous amplitude comparison technique for target elevation-angle determination derive the elevation angle inside the radar beamwidth by measuring the ratio of simultaneous signal returns on two squinted received beams after having illuminated the target in some manner. The resulting elevation-angle data is independent of the manner in which the target is illuminated by the radar and is dependent only on the squinted *receiving*-antenna patterns.

In analyzing the elevation-angle errors due to ground reflections, we shall consider the case where the boresight crossover of a pair of squinted receiving beams (*A* and *B*) is oriented exactly on the target at elevation angle θ (a condition of zero error in the absence of ground reflections). See Fig. 20.9.

With pattern functions of beams *A* and *B* assumed to be identical and with the centerlines of beams *A* and *B* oriented at elevation angles of $\theta - \alpha$ and $\theta + \alpha$, respectively, the net received field strength at the feed points of beams *A* and *B* (relative to the peak of each beam) is then

*The material in this subsection was originally written by Burt Brown and appeared in Sec. 22.3 of the first edition of the handbook.

$$E_A = E_{A(\alpha)} + KE_{A(2\theta-\alpha)}e^{-j(\phi+2D\sin\theta)}$$
$$E_B = E_{B(\alpha)} + KE_{B(2\theta+\alpha)}e^{-j(\phi+2D\sin\theta)} \tag{20.21}$$

where K = amplitude of reflection coefficient
ϕ = phase of reflection coefficient
$E_{A(\alpha)} = E_{B(\alpha)}$ = relative received field strength of beams A and B from signal arriving along direct path at angle α from peaks of beams A and B
$E_{A(2\theta-\alpha)}$ = relative received field strength of beam A from reflected path at $2\theta - \alpha$ from peak of beam A
$E_{B(2\theta+\alpha)}$ = relative received field strength of beam B from reflected path at $2\theta + \alpha$ from peak of beam B

The magnitude of the off-boresight elevation-angle error due to ground reflections is a function of the ratio of the magnitudes of E_A and E_B, or

$$\text{Elevation error} = f\frac{|E_A|}{|E_B|} = f\frac{|E_{A(\alpha)} + KE_{A(2\theta-\alpha)}e^{-j(\phi+2D\sin\theta)}|}{|E_{B(\alpha)} + KE_{B(2\theta+\alpha)}e^{-j(\phi+2D\sin\theta)}|} \tag{20.22}$$

When $KE_{A(2\theta-\alpha)}$ and $KE_{B(2\theta+\alpha)}$ are small compared with $E_{A(\alpha)}$, the maximum value of $f(|E_A|/|E_B|)$ is equal to

$$\frac{E_{A(\alpha)} + KE_{A(2\theta-\alpha)}}{E_{B(\alpha)} - KE_{B(2\theta+\alpha)}} \tag{20.23}$$

To illustrate these effects, a specific example is cited where the amplitude comparison beams A and B are assumed to have the following characteristics:

Antenna aperature (α) = 25.5λ

$$\text{Receiving beam pattern function} \frac{\sin[\pi(\alpha/\lambda)\sin\theta]}{\pi(\alpha/\lambda)\sin\theta} = \frac{\sin(25.5\pi\sin\theta)}{25.5\pi\sin\theta}$$

Beamwidth (at -3 dB points) = 2.0°

Squint angle (α) = 1.125°

Antenna height above ground = 50λ

The ground-reflection coefficient $Ke^{j\Phi}$ is assumed to be $1.0e^{j\pi}$, which corresponds to horizontal polarization over an infinite conducting plane.

With these values, Fig. 20.10 shows a plot of the resultant relative field strengths in beams A and B as a function of the elevation boresight pointing angle θ. Note that in these curves, for each value of elevation angle θ, the antenna boresight is assumed to be directed exactly on the target. Thus, in the *absence* of ground reflections, the net field strengths in A and B would have been *equal* for all values of θ.

The corresponding off-boresight errors for the amplitude curves of Fig. 20.10 are shown in Fig. 20.11. In viewing the characteristics of the off-boresight error curves of Fig. 20.11, the important features to be noted are as follows:

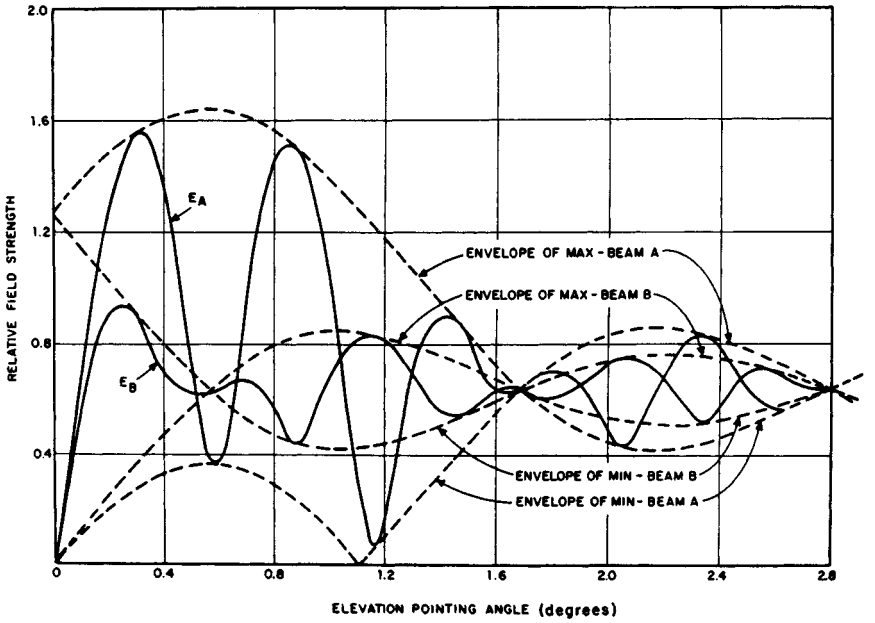

FIG. 20.10 Resultant relative field strength received in beams *A* and *B* resulting from ground reflections as a function of the elevation pointing angle of the beam crossover. Beamwidth is 2°; antenna height, 50λ; total squint angle, 2.25°; and reflection coefficient, 1.0.

1. The shape and amplitude of the *envelope of maximum errors* (dash curves) are dependent only on the antenna-beam pattern function in the elevation plane and the ground-reflection coefficient and are independent of the antenna electrical height above the ground.

2. The configuration of the error curve lying inside the envelope of maximum errors (i.e., the positions and spacing of the peak errors) is dictated chiefly by the antenna electrical height above the ground (in wavelengths) and, to a minor extent, by the phase angle of the antenna sidelobes that receive the reflected rays.

A similar analysis can be made of the errors due to surface reflections for a simultaneous phase comparison system, as found in Sec. 22.3 of the first edition of this handbook.

At high elevation pointing angles, where the errors are due only to surface reflections from the negative elevation-angle sidelobes, the errors contributed by various sidelobe levels in simultaneous amplitude comparison and phase comparison radars may be summarized approximately as follows: 0.2 to 0.3 beamwidth, when the surface-reflected sidelobe is 10 dB down from the peak; 0.07 to 0.10 beamwidth for −20 dB sidelobes; 0.025 to 0.035 for −30 dB sidelobes; 0.008 to 0.011 for −40 dB sidelobes; and about 0.003 beamwidth for −50 dB sidelobes illuminating the surface.

Low-Angle Squinted-Beam Height Finding. One height finding technique which has proved practical and effective against surface multipath is the so-called low-angle squinted-sum-beam height finding technique employed in the

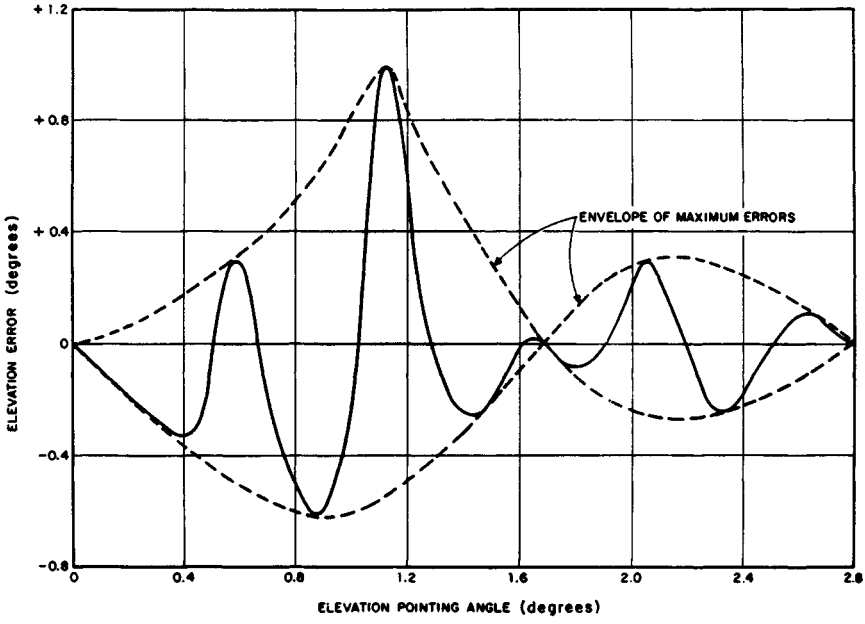

FIG. 20.11 Elevation errors due to ground reflection as a function of pointing angle for amplitude comparison system and uniform aperture distribution. Other conditions are as in Fig. 20.10.

TPS-59/GE-592/FPS-117 solid-state radar series.[27] The problem with conventional sum-delta monopulse in a surface multipath environment is that the delta-beam peak response is in the direction of the indirect-path reflection. The low-angle technique avoids this problem by using a pair of squinted beams on receive, as illustrated in Fig. 20.12. The lower beam, unweighted so as to generate as narrow a beam as permitted by the array aperture, is placed in elevation so that the indirect path is attenuated by the lower side of the beam. The upper beam, weighted to produce low sidelobes, is placed a degree or so above the lower beam so that the indirect-path echo is rejected by the sidelobes of the upper beam while the direct-path echo is received at high gain. This approach tends to minimize the amount of indirect-path energy in the two beams while maintaining coverage on the horizon.

The performance of the low-angle squinted-sum-beam technique also differs from that of a conventional stacked-beam pair, for two reasons. First, the two receive beams in the low-angle technique are not formed from identical aperture illuminations. Second, the transmit beam in the low-angle technique is narrow, reducing indirect multipath returns and to a lesser degree off-boresight signal-to-noise ratio.

The performance of a version of the low-angle squinted-sum-beam technique relative to that of a conventional monopulse is compared in Fig. 20.13 for a surface reflection coefficient of -1, approximately that of a smooth sea. The antenna in each case is situated at a height of twice the vertical aperture dimension above a flat earth. The monopulse case consists of a uniformly illuminated sum beam and a half-aperture uniform difference beam electronically phase-steered to $u_0 = 0.5$, processed, and implemented with full vector processing. The low-angle

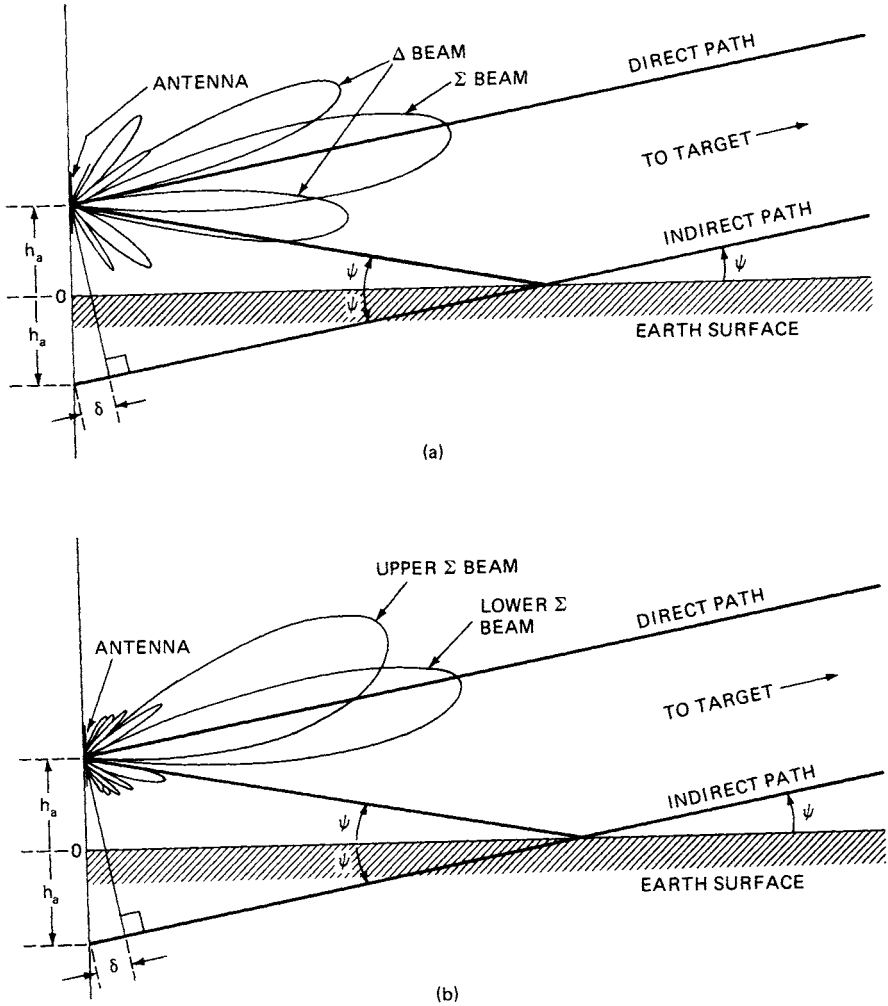

FIG. 20.12 Multipath impact on monopulse; δ = path difference. (*a*) Conventional sum-delta monopulse. (*b*) Squinted-sum-beam low-angle technique.

technique examined consists of a uniformly illuminated transmit/receive lower beam, accompanied by a weighted aperture upper beam. The lower beam is electronically phase-steered to $u_1 = 0.5$ while the upper beam is electronically phase-steered an additional $\delta u = 1.0$ (i.e., to $u_2 = 1.5$). This places the multipath largely in the sidelobe of the upper beams. In the monopulse case, the multipath introduces severe bias errors into the elevation-angle estimate with peaks on the order of 0.4 in u space. For a radar with an aperture of $L/\lambda = 32$, this corresponds to an rmse of 12.5 msines. The multipath bias errors dominate the total accuracy performance of the monopulse technique and, contrary to the behavior of the thermal errors, are not suppressed by high target signal-to-noise ratios. By

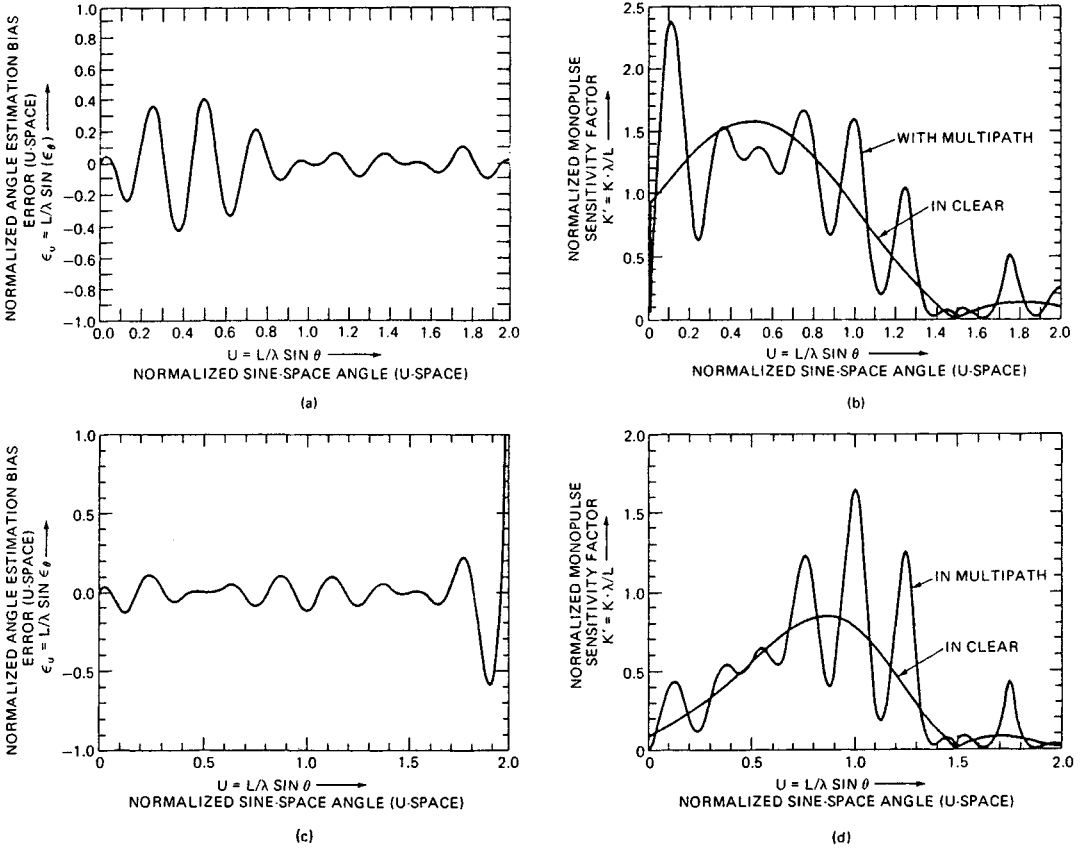

FIG. 20.13 Accuracy comparison in multipath. (*a*) Sum-delta monopulse bias error. Antenna height = 2 × aperture height; monopulse beams boresighted at $u_0 = 0.5$; reflection coefficient = − 1. (*b*) Sum-delta monopulse sensitivity factor. Antenna height = 2 × aperture height; monopulse beams boresighted at $u_0 = 0.5$; reflection coefficient = − 1. (*c*) Squinted-sum low-angle bias error. Antenna height = 2 × aperture height; lower beam boresighted at $u_0 = 0.5$; upper beam boresighted at $u_1 = 1.5$; reflection coefficient = − 1. (*d*) Squinted-sum low-angle sensitivity factor. Antenna height = 2 × aperture height;

contrast, the bias errors introduced by the multipath in the low-angle squinted-sum-beam technique are kept to peaks on the order of 0.15 in u space, corresponding to an rmse of approximately 4.7 msines for a radar of the same aperture. Further reduction might be possible with an optimization of the beam placement and aperture illumination functions.

REFERENCES

1. Skolnik, M. I.: Fifty Years of Radar, *Proc. IEEE*, vol. 73, pp. 182–197, February 1985.
2. Guerlac, H. E.: "Radar in World War II," Tomash Publishers, American Institute of Physics, Los Angeles, 1987.
3. Ridenour, L. N.: "Radar System Engineering," MIT Radiation Laboratory Series, vol. 1, McGraw-Hill Book Company, New York, 1947.
4. The SCR-268 Radar, *Electronics*, vol. 18, pp. 100–109, September 1945.
5. The SCR-584 Radar, *Electronics*, vol. 18, pp. 104–109, November 1945.
6. Schneider, E. G.: Radar, *Proc. IRE*, vol. 34, pp. 528–578, August 1946.
7. Brookner, E.: "Radar Technology," Artech House, Norwood, Mass., 1980, pp. 5–59.
8. Sutherland, J. W.: Marconi S600 Series of Radars, *Interavia*, vol. 23, pp. 73–75, January 1968.
9. Skolnik, M. I.: "Introduction to Radar Systems," 2d ed., McGraw-Hill Book Company, New York, 1980.
10. Brown, B. P.: Radar Height Finding, chap. 22 of Skolnik, M. I. (ed.): "Radar Handbook," 1st ed., McGraw-Hill Book Company, New York, 1970.
11. Simpson, T. J.: The Air Height Surveillance Radar and Use of Its Height Data in a Semi-Automatic Air Traffic Control System, *IRE Int. Conv. Rec.*, vol. 8., pt. 8, pp. 113–123, 1960.
12. Watanabe, M., T. Tamana, and N. Yamauchi: A Japanese 3-D Radar for Air Traffic Control, *Electronics*, p. 68, June 21, 1971.
13. AN/TPS-43E Tactical Radar System, brochure, Westinghouse Corporation.
14. The Martello High Power 3-D Radar System, brochure, Marconi Company.
15. RAT-31S 3D Surveillance Radar, brochure, Selenia Radar and Missile Systems Division, Rome.
16. Hammer, I. W.: Frequency-Scanned Arrays, chap. 13 of Skolnik, M. I. (ed.): "Radar Handbook," 1st ed., McGraw-Hill Book Company, New York, 1970.
17. Milne, K.: The Combination of Pulse Compression with Frequency Scanning for Three Dimensional Radars, *Radio Electron. Eng.*, vol. 28, pp. 89–106, August 1964.
18. Polmar, N.: "Ships and Aircraft of The U.S. Fleet," 14th ed., Naval Institute Press, Annapolis, Md., 1987, chap. 29, Electronic Systems.
19. AR-3D Mobile Air Defense Radar System, brochure, Plessey.
20. Pretty, R. T. (ed.): "Jane's Weapon Systems, 1981–1982," pp. 449–596.
21. Pfister, G.: The Series 320 Radar, Three Dimensional Air Surveillance Radar for the 1980's, *IEEE Trans.*, vol. AES-16, pp. 626–638, September 1980.
22. Lain, C. M., and E. J. Gersten: AN/TPS-59 System, *IEEE Int. Radar Conf. Rec.*, IEEE Publ. 75 CHO 938-1 AES, pp. 527–532, Apr. 21–23, 1975.
23. AN/TPS-59 Tactical Solid State Radar, brochure, General Electric Company.

24. AN/TPS-59: First Total Solid State Radar, *ADCOM Commun. Electron. Comput. Resources Dig.* (editorial article), October–November–December 1976.
25. AN/FPS-117 Minimally Attended Solid State Radar System, brochure, General Electric Company.
26. Gostin, J. J.: The GE592 Solid State Radar, *EASCON '80 Rec.*, pp. 197–203, IEEE Publ. 80 Ch 1578-4 AES, Sept. 29, 30, Oct. 1, 1980.
27. GE-592 Solid State Radar Systems, brochure, General Electric Company.
28. Klass, P. J.: Solid State 3D Radar for NATO Tested, *Aviat. Week Space Technol.*, May 21, 1979.
29. U.S. Air Force reports on Hughes Air Defense Radar, *Flight Int.*, Dec. 4, 1982.
30. Smith, E. K., and S. Weintraub: The Constraints in the Equation for Atmospheric Refractive Index at Radio Frequencies, *Proc. IRE*, vol. 41, pp. 1035–1037, August 1953.
31. Blake, L. V.: Ray Height Computation for a Continuous Nonlinear Atmospheric Refractive-Index Profile, *Radio Sci.*, vol. 3, pp. 85–92, January 1968.
32. Millman, G. H.: Atmospheric Effects on Radio Wave Propagation, in Berkowitz, R. S. (ed.): "Modern Radar Analysis, Evaluation and System Design," John Wiley & Sons, New York, 1965, pp. 315–377.
33. Bean, B. R., and E. J. Dutton: Radio Meteorology, *Nat. Bur. Stand. Monog.* 92, pp. 59–76, March 1966.
34. Bauer, J. R., W. C. Mason, and R. A. Wilson: Radio Refraction in a Cool Exponential Atmosphere, *MIT Lincoln Laboratory, Tech. Rept.* 186, August 1958.
35. Bauer, J. R., and R. A. Wilson: Precision Tropospheric Radio Refraction Corrections for Ranges from 10–500 Nautical Miles, *MIT Lincoln Laboratory, Rept.* 33G-0015, Feb. 20, 1961.
36. Sherman, S. M.: "Monopulse Principles and Techniques," Artech House, Norwood, Mass., 1985, chap. 5, chap. 12, pp. 345–348.
37. Rhodes, D. R.: "Introduction to Monopulse," McGraw-Hill Book Company, New York, 1959; reprinted by Artech House, Norwood, Mass., 1982.
38. Kinsey, R. R.: Monopulse Difference Slope and Gain Standards, *IRE Trans.*, vol. AP-10, pp. 343–344, May 1962.